JOURNAL OF GEOPHYSICAL RESEARCH: PLANETS, VOL. 118, 1397–1413, doi:10.1002/jgre.20101, 2013

Band-limited Bouguer gravity identifies new basins on the Moon

W. E. Featherstone,[1] C. Hirt,[1] and M. Kuhn[1]

Received 7 November 2012; revised 30 May 2013; accepted 2 June 2013; published 28 June 2013.

[1] Spectral domain forward modeling is used to generate topography-implied gravity for the Moon using data from the Lunar Orbiter Laser Altimeter instrument operated on board the Lunar Reconnaissance Orbiter mission. This is subtracted from Selenological and Engineering Explorer (SELENE)-derived gravity to generate band-limited Bouguer gravity maps of the Moon so as to enhance the gravitational signatures of anomalous mass densities nearer the surface. This procedure adds evidence that two previously postulated basins on the lunar farside, Fitzgerald-Jackson (25°N, 191°E) and to the east of Debye (50°N, 180°E), are indeed real. When applied over the entire lunar surface, band-limited Bouguer gravity reveals the locations of 280 candidate basins that have not been identified when using full-spectrum gravity or topography alone, showing the approach to be of utility. Of the 280 basins, 66 are classified as distinct from their band-limited Bouguer gravity and topographic signatures, making them worthy of further investigation.

Citation: Featherstone, W. E., C. Hirt, and M. Kuhn (2013), Band-limited Bouguer gravity identifies new basins on the Moon, *J. Geophys. Res. Planets*, *118*, 1397–1413, doi:10.1002/jgre.20101.

1. Introduction

[2] Understanding the structure and evolution of the Moon has benefitted greatly from satellite-based topographic mapping and satellite-based gravimetry. For instance, there are (i) asymmetry between the nearside and the farside hemispheres with a ~1.9 km offset between the center of figure (from topography) and the center of mass (from gravimetry) [*Smith et al*., 1997], (ii) the early detection of "mascons" [*Muller and Sjogren*, 1968], and (iii) information on the long-wavelength isostatic compensation state of the lunar crust [e.g., *Wieczorek*, 2007]. Overviews of the various lunar satellite missions are given in, e.g., *Floberghagen* [2002], *Matsumoto et al*. [2010], *Sinha et al*. [2010], *Vondrak et al*. [2010], and *Zuber et al*. [2013].

[3] Early satellite-based studies of the farside had previously been hampered by the inability to track lunar-orbiting satellites from the Earth due to the synchronous rotation and revolution of the Moon. This was redressed by the Selenological and Engineering Explorer (SELENE) lunar gravity mission [e.g., *Namiki et al*., 2009], which has already revealed several new features on the farside. Most of these are large-scale basins because smaller structures could not be discriminated from noise in the high-degree spherical harmonic coefficients of the SGM100h gravity model [e.g., *Matsumo et al*., 2010]. In addition, small-scale structures can be obscured by the long-wavelength gravitational signatures.

[1]Western Australian Centre for Geodesy and Institute for Geoscience Research, Curtin University of Technology, Perth, Western Australia, Australia.

Corresponding author: W. E. Featherstone, Western Australian Centre for Geodesy and Institute for Geoscience Research, Curtin University of Technology, GPO Box U1987, Perth, WA 6845, Australia. (w.featherstone@curtin.edu.au)

2169-9097/13/10.1002/jgre.20101

[4] In this article, we instead compute band-limited Bouguer gravity (BGG) from the newer SGM100i gravity model [*Goossens et al*., 2011] and LOLA (Lunar Orbiter Laser Altimeter) topography [*Smith et al*., 2010]. This reveals basins that were previously masked when using full-spectrum Bouguer gravity from SELENE alone [cf. *Matsumoto et al*., 2010] or topography alone [cf. *Frey*, 2011]. We present three case studies to exemplify: (i) the masking when using full-spectrum Bouguer gravity on its own, (ii) validation of the band-limited approach using an already known lunar basin, and (iii) adding more evidence for the presence of two farside basins [Fitzgerald-Jackson (25°N, 191°E) and to the east of Debye (50°N, 180°E)] using band-limited Bouguer gravity. Sensitivity analyses are conducted by varying the topographic mass density used in the forward modeling and the degrees of band limitation, indicating these identifications to be robust.

[5] The band-limited Bouguer gravity technique is then extended to the entire lunar surface, corroborating the presence of small-scale (~100 km to ~300 km in diameter) basins: Some are already known, some are probable, and some are uncertain but remain candidates for future investigations.

2. Methods and Data

[6] *Namiki et al*. [2009], *Matsumoto et al*. [2010], and several others generally use full-spectrum Bouguer gravity, where the spherical harmonic summations of gravity and topography begin at degree $n = 2$. The method used in this paper starts the summations in equations (1) and (4) at arbitrarily higher degrees ($n1 > 2$), thus enhancing the medium- and shorter-wavelength signals that are generated by near-surface mass anomalies (section 2.3). However, both methods are inevitably restricted by the maximum reliable degree of the lunar gravitational model and noise in the high-degree coefficients.

[7] The use of band-limited data in the planetary sciences is not novel, however. For instance, *Frey et al.* [1996] correlated band-limited free-air gravity with topography-implied gravity in spherical harmonic bands on Mars. *Han* [2008] used high-pass-filtered free-air gravity in the context of localized spherical harmonic functions on the Moon. *Zuber et al.* [2013] emphasized shorter-scale Bouguer gravity signatures through high-pass filtering, also on the Moon. However, band-limited Bouguer gravity is not used routinely in practice. Finally, we note that the band-limited approach is conceptually quite similar to regional-residual separation that has been applied to Bouguer gravity on Earth [e.g., *Griffin*, 1949; *Nettleton*, 1954].

2.1. Band-Limited Gravity From Lunar Gravitational Models

[8] Spherical harmonic syntheses of SGM100i are used to generate band-limited lunar gravity disturbances, which are synonymously termed radial derivatives of the gravitational potential in the planetary science literature [e.g., *Wieczorek*, 2007, p. 6]; this is

$$\left[\delta g_{n1}^{n2}\right]_{\mathrm{SGM}} = \frac{GM}{r^2}\sum_{n=n1}^{n2}\left(\frac{R}{r}\right)^n (n+1)\sum_{m=0}^{n} \left(\overline{C}_{nm}\cos m\lambda + \overline{S}_{nm}\sin m\lambda\right)\overline{P}_{nm}(\cos\theta) \tag{1}$$

where $GM = 4902.80080 \times 10^9\ \mathrm{m^3\ s^{-2}}$ [*Goossens et al.*, 2011] is the product of the universal gravitational constant G and the lunar mass M for SGM100i, r is the selenocentric radius to the computation point, $R = 1{,}738{,}000$ m is the SGM100i model's reference radius, $n1$ and $n2$ denote the lower and upper degrees of the band-limited syntheses, $\overline{C}_{nm}$ and $\overline{S}_{nm}$ are the fully normalized coefficients of SGM100i (from http://www.miz.nao.ac.jp/rise-pub/en), $\overline{P}_{nm}(\cos\theta)$ are the fully normalized associated Legendre functions, and θ and λ are, respectively, the colatitude and longitude of the computation point. The $(n+1)$ term in equation (1) delivers gravity disturbances, whereas $(n-1)$ delivers gravity anomalies, which will be discussed further below. SGM100i is provided to degree $n_{\max} = 100$, but *Goossens et al.* [2011] recommend that it only be used to degree 70 because of noise in the higher-degree coefficients. As such, all syntheses herein are limited to $n2 = 70$.

[9] For computational speed and consistency with other works on planetary gravimetry, we have evaluated equation (1) at the surface of the SGM100i model's reference sphere of radius $r = R = 1{,}738{,}000$ m. The use of some constant reference radius r, often set equal to the gravity model's radius R, follows common practice in the planetary sciences [e.g., *Konopliv et al.*, 2001; *Wieczorek*, 2007; *Matsumoto et al.*, 2010]. We acknowledge that this raises the problem of gravity continuation when r is inside the topographic masses. Alternatively, gravity can be evaluated at the surface of the topography [cf. *Hirt*, 2012], thus avoiding the need to take into account these additional continuation terms [e.g., *Sjöberg*, 2007]. We experimented with both cases, and it did not affect the spatial mapping of the basins.

[10] The subtle difference between gravity anomalies and gravity disturbances is described by, e.g., *Hackney and Featherstone* [2003a]. In short, the disturbance is the difference between model gravity and reference gravity evaluated at exactly the same point, and the anomaly is the difference evaluated at different points. However, the use of anomalies or disturbances has little consequence here, as we are seeking to locate the basins, rather than apply the subtleties of geodetic approaches and terminology to the planetary sciences. Hereafter, we simply use the term "gravity" to denote the radial derivatives of the gravitational potential at $r = R$ from equation (1).

2.2. Band-Limited Gravity From Lunar Topography

[11] The lunar topography model used herein comes from the 2010 release produced by the LOLA instrument on board the Lunar Reconnaissance Orbiter (LRO) mission [*Vondrak et al.*, 2010]. The LRO configuration delivers an ~18 m along-track and an ~1.8 km across-track spacing at the equator [*Smith et al.*, 2010]. The $\overline{HC}(p)_{nm}$ and $\overline{HS}(p)_{nm}$ coefficients were taken from http://pds-geosciences.wustl.edu/lro/lro-l-lola-3-rdr-v1/lrolol_1xxx/data/lola_shadr/ (version lro_ltm02_sha.tab), which are based on around 1 year of LOLA observations (start date: 13 July 2009; end date: 20 August 2010) (G. Neumann, personal communication, 2013). While the maximum spherical harmonic degree available is 719, it has been truncated to degree 70 so as to be consistent with the maximum reliable degree of SGM100i.

[12] Band-limited spectral domain forward modeling was used to generate gravity from the LOLA lunar topography. We have validated this spectral approach with brute force numerical integration of band-limited topography, with both approaches giving comparable results. The fully normalized spherical harmonic coefficients of the gravitational potential of the topography are obtained from [e.g., *Rummel et al.*, 1988; *Wieczorek and Phillips*, 1998]

$$\begin{Bmatrix}\overline{C}_{nm}^{\mathrm{TIG}}\\ \overline{S}_{nm}^{\mathrm{TIG}}\end{Bmatrix} = \frac{4\pi}{2n+1}\frac{R^2}{M}\rho\sum_{p=1}^{p_{\max}}\frac{\prod_{q=1}^{p}(n+4-q)}{p!(n+3)}\begin{Bmatrix}\overline{HC}(p)_{nm}\\ \overline{HS}(p)_{nm}\end{Bmatrix} \tag{2}$$

where $p_{\max}$ is the order of the series expansion, M is the lunar mass (7.347×10^{22} kg, derived from GM/G for SGM100i), ρ is the assumed mass density of the lunar topography, and $\overline{HC}(p)_{nm}$ and $\overline{HS}(p)_{nm}$ are derived from spherical harmonic analysis of the surface function

$$H(p) = \frac{H^p}{R^{p-1}} \tag{3}$$

where H is the height of the LOLA topography relative to the reference sphere of radius $R = 1{,}737{,}400$ m. The 600 m difference in reference radii between SGM100i and LOLA results in a direct current (DC) shift of Bouguer shell gravity of 134.28 mGal, computed from $4\pi G\rho H$. However, this constant term does not affect the spatial mapping of the basins. The coefficients from equation (2) are converted to band-limited topography-implied gravity using

$$\left[\delta g_{n1}^{n2}\right]_{\mathrm{TIG}} = \frac{GM}{R^2}\sum_{n=n1}^{n2}(n+1)\sum_{m=0}^{n} \left(\overline{C}_{nm}^{\mathrm{TIG}}\cos m\lambda + \overline{S}_{nm}^{\mathrm{TIG}}\sin m\lambda\right)\overline{P}_{nm}(\cos\theta) \tag{4}$$

[13] The approximation error arising from truncating the series expansion in equation (2) decreases with increasing

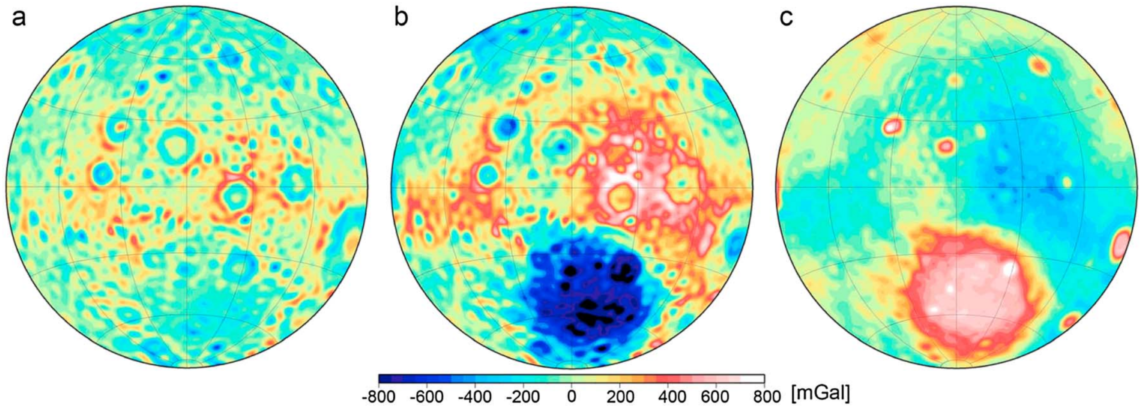

Figure 1. (a) Full-band SGM100i gravity, (b) full-band topography-implied gravity, and (c) full-band Bouguer gravity. Units in mGal. All panels show the lunar farside.

order $p_{\max}$. *Wieczorek* [2007] found that $p_{\max} = 4$ [and $n_{\max} \leq 90$] gives rise to maximum errors of <1 mGal anywhere on the Moon, which is about two orders of magnitude less than the band-limited Bouguer gravity (sections 3 and 4). In this study, we have evaluated equation (2) for $p_{\max} = 5$, which makes the approximation error even smaller. Equation (2) also relies on a constant mass density assumption, which we shall investigate later (section 3) by evaluating it for two likely end-members of the lunar topographic mass density.

[14] The band-limited Bouguer gravity is then computed as equation (1) minus equation (4) but only for the same values of $n1 > 2$ and $n2 \leq n_{\max}$. Equations (1) and (4) also omit the degree-1 term of the topography which results from the ~1.9 km offset between the Moon's center of mass and center of figure, but this manifests as a very long wavelength signal that we wish to remove to enhance the detailed gravity signatures.

2.3. Selection of Bandwidths

[15] We have used two criteria to select the bandwidths of the Bouguer gravity used for the identification of lunar basins: (i) the limiting relation of *Bowin* [1983], which gives the deepest point mass that can generate a surface spherical harmonic signature of a particular degree n; and (ii) the typical spatial scale of the basins versus the maximum reliable degree of the gravity model, which is $n2 = 70$ in the case of SGM100i. However, interpretation of gravity data is inherently plagued by nonuniqueness. For instance, a lens-shaped mass anomaly near the surface can generate the same gravitational signature as a deeper point mass.

[16] *Bowin*'s [1983] limiting relation is given by

$$Z_n = \frac{R}{(n-1)} \tag{5}$$

where Z_n is the maximum depth of the point mass that generates a surface feature of degree n (and R is the mean spherical radius of the Moon). There is also a relation between the degree n of a feature and its spatial scale s of a spherical body; this is

$$s = \frac{\lambda_{\min}}{2} = \frac{\pi R}{n} \tag{6}$$

[17] For instance, starting the summations in equations (1) and (4) at $n1 = 18$ senses spatial scales shorter than ~300 km and point masses no deeper than ~100 km. In equation (6), we also distinguish between s and the minimum resolvable wavelength $\lambda_{\min}$.

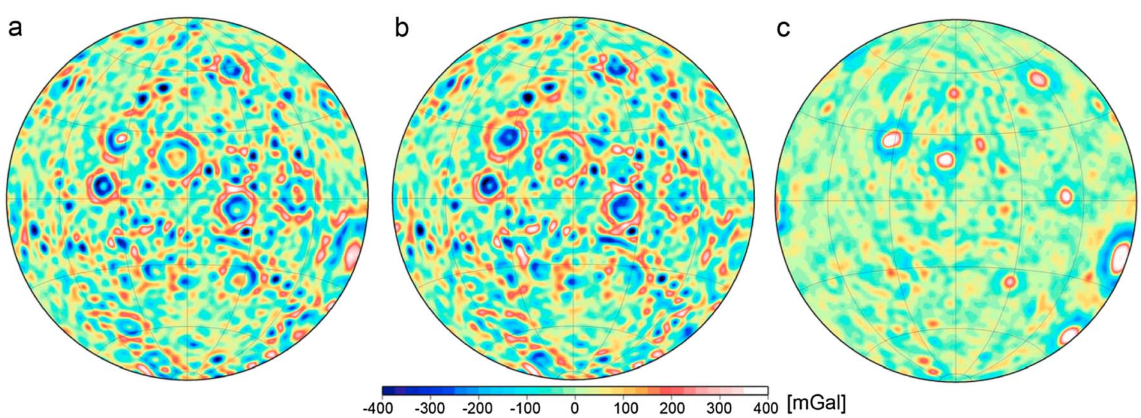

Figure 2. (a) Band-limited SGM100i gravity, (b) band-limited topography-implied gravity, and (c) band-limited Bouguer gravity. Units in mGal. The spectral band is $n1 = 18$ to $n2 = 70$, corresponding to spatial scales between ~300 km and ~80 km and a limiting depth of ~100 km. All panels show the lunar farside.

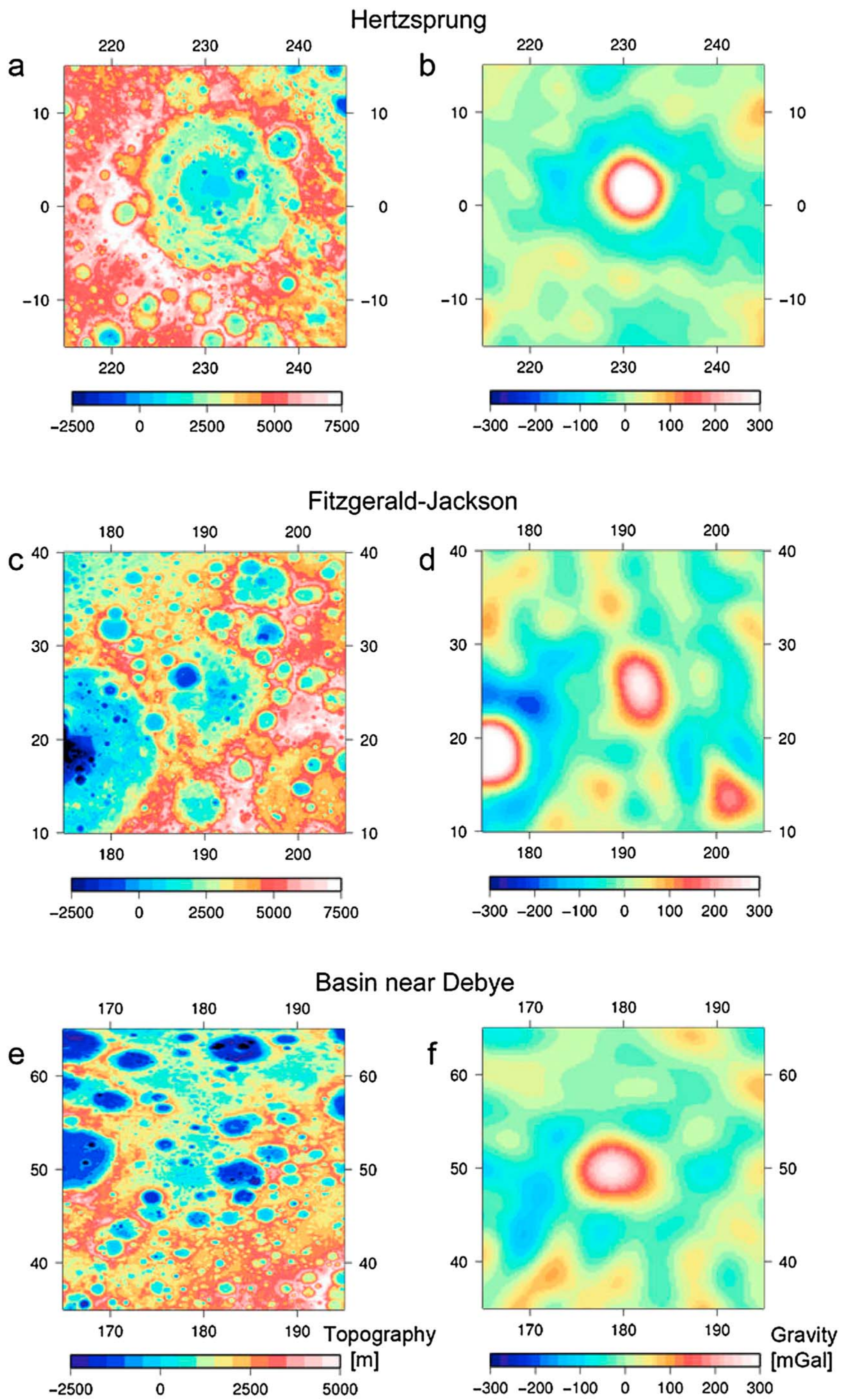

Figure 3. (a, c, e) LOLA topography in meters and (b, d, f) band-limited Bouguer gravity in mGal for the three selected farside regions: Hertzsprung is shown in Figures 3a and 3b, Fitzgerald-Jackson is shown in Figures 3c and 3d, and the basin near Debye is shown in Figures 3e and 3f. The spectral band is $n1 = 18$ to $n2 = 70$, corresponding to spatial scales between ~300 km and ~80 km and a limiting depth of ~100 km.

[18] This band-limited approach also lessens the influence of assumptions about lunar isostatic compensation on our mapping. For instance, *Sugano and Heki* [2004] assert that there is no isostatic compensation for lunar basins with diameters up to 300 km. This is contradicted somewhat by *Reindler and Arkani-Hamed* [2001], who state that "most intermediate-size lunar craters show some degree of compensation." However, the aim of this investigation is more concerned with the identification and spatial location of basins rather than interpretations of their isostatic state.

3. Exemplar Studies

[19] As stated, the computation of lunar gravity is most often performed over all spatial scales, e.g., to the maximum available expansion of the model. We therefore first present

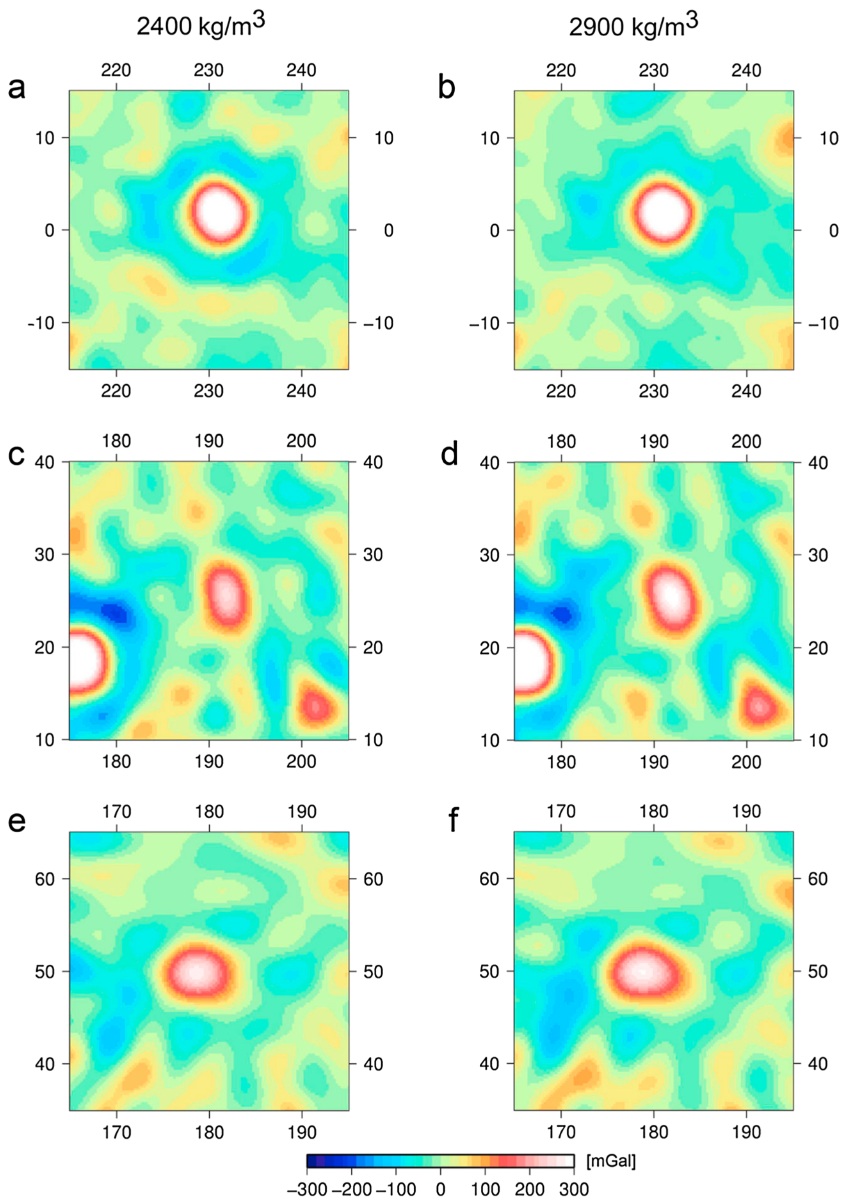

Figure 4. Band-limited Bouguer gravity (a, c, e) based on a mass density of 2400 kg m^{-3} and (b, d, f) based on 2900 kg m^{-3}. Hertzsprung is shown in Figures 4a and 4b, Fitzgerald-Jackson is shown in Figures 4c and 4d, and the basin near Debye is shown in Figures 4e and 4f. The spectral band is $n1 = 18$ to $n2 = 70$, corresponding to spatial scales between ~300 km and ~80 km and a limiting depth of ~100 km.

full-band Bouguer gravity derived from SGM100i and LOLA (lro_ltm02_sha.tab) as a slightly updated replication of the farside results in *Matsumoto et al.* [2010] and *Namiki et al.* [2009]. That is, equations (1) and (4) are evaluated from $n1 = 2$ to $n2 = 70$, the degree to which SGM100i contains full power [*Goossens et al.*, 2011]. In this initial example, the topography-implied gravity has been computed using a constant mass density assumption of 2700 kg m^{-3}, which is taken as the most representative topographic mass density of the farside topography from pre–Gravity Recovery and Interior Laboratory (GRAIL) values given in *Huang and Wieczorek* [2012], but a sensitivity analysis incorporating the more recent GRAIL-derived mass densities [cf. *Wieczorek et al.*, 2013] will be presented later in this section.

[20] Figure 1a shows full-banded gravity from SGM100i to $n2 = 70$ (equation (1)), Figure 1b shows the topography-implied gravity, spectrally forward modeled from the LOLA topography over the same bands (equations (2)–(4)), and Figure 1c shows their difference which is the full-banded Bouguer gravity. Comparing Figure 1c with *Matsumoto et al.* [2010, Figure 12] shows that two farside features are better resolved by the SGM100i gravity model: Fitzgerald-Jackson (25°N, 191°E) and what could possibly be a basin to the east of Debye at 50°N, 180°E. These two features can only just be discriminated in *Matsumoto et al.* [2010, Figure 12] with the benefit of hindsight, but the noise in SGM100h and its expansion to degree 100 cause a cantaloupe effect that renders them uncertain in *Matsumoto et al.* [2010].

Table 1. Spatial Resolution and Limiting Depth Corresponding to Different Spherical Harmonic Degrees (Computed From Equations (6) and (5))

Degree	Spatial Resolution (km)	Limiting Depth (km)
5	~1100	~430
10	~550	~190
25	~220	~70
36	~150	~50
70	~80	~25

[21] To achieve improved mapping of basins where the planetary gravity field and topography have been observed, we propose the use of band-limited Bouguer gravity because it is capable of emphasizing the signatures of regional and near-surface mass density anomalies (section 2.3). The benefits of this strategy are exemplified here for SGM100i gravity mapping of selected features over the lunar farside. As a first case study example, we use SGM100i and topography-implied gravity in the spectral band between degrees $n1 = 18$ and $n2 = 70$. This corresponds to spatial scales from ~300 km to ~80 km (equation (5)) and a limiting depth of the generating mass anomalies of ~100 km (equation (6)). Of course, other parameters can be selected according to the analyst's choice.

[22] Figure 2c shows that the band-limited Bouguer approach enhances the gravity signatures of many farside basins occurring at spatial scales less than ~300 km. Notably, the clear signature of the massive South Pole-Aitken Basin in Figure 1c is absent from Figure 2c, showing the high-pass spatial filtering effect of the band-limited approach. It also much enhances the signatures of Fitzgerald-Jackson (25°N, 191°E) and the basin at 50°N, 180°E. Most basins are characterized by central positive gravity highs, surrounded by annular gravity lows. They are also more distinct in comparison to the SGM100i gravity alone (cf. Figures 1a, 2a, and 2c). Hence, band-limited gravity emphasizes the basin signatures much better than the full-spectrum Bouguer gravity maps.

[23] In the remainder of this section, we focus on three farside basins: Hertzsprung (centered at 1.5°N, 128.5°W), Fitzgerald-Jackson (centered at 25°N, 191°E), and the basin to the east of Debye centered at 50°N, 180°E. We use Hertzsprung to validate the band-limited technique because it is a well-established impact basin on the more challenging farside. *Huang et al.* [2009] and *Frey* [2011] postulated the

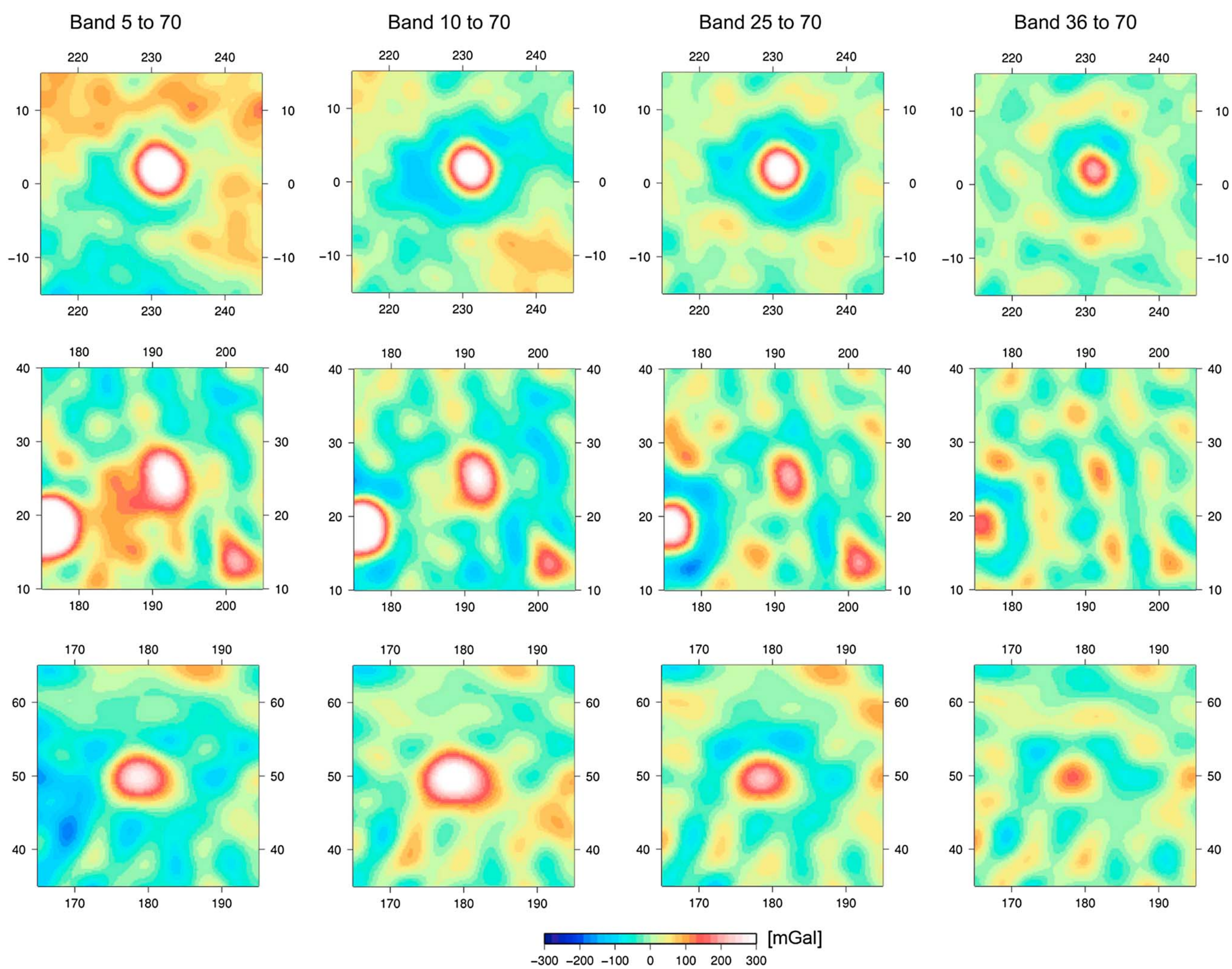

Figure 5. Band-limited Bouguer gravity for various spectral bands. (top) Hertzsprung, (middle) Fitzgerald-Jackson, and (bottom) the basin near Debye. The spatial scales and limiting depths for each band are given in Table 1.

Table 2. Classification of Previously Reported Lunar Basins Based on Band-Limited Bouguer Gravity[a]

Basin Identification[b]					Band-Limited Bouguer Gravity							References[h]
Name	Symbol	Lat (°)	Lon (°)	*D* (km)	gr[c]	*r*[d]	tr[e]	Rating 1[f]		Rating 2[g]		
Crisium	Cr	17.5	58.5	1060	3	3	3	9	Distinct	6	Distinct	1,2,4
Orientale	Or	−20.0	265.0	930	3	3	3	9	Distinct	6	Distinct	1,2,3,4
Mendel-Rydberg	MR	−50.0	266.0	630	3	3	3	9	Distinct	6	Distinct	1,2,3,4
Humboldtianum[i]	Hm	61.0	84.0	600	3	3	3	9	Distinct	6	Distinct	1,2,3,4
Freundlich-Sharonov	FS	18.5	175.0	600	3	3	3	9	Distinct	6	Distinct	1,2,3,4
Hertzsprung	He	1.5	231.5	570	3	3	3	9	Distinct	6	Distinct	1,2,3,4
Nectaris	Ne	−16.0	34.0	860	3	3	2	8	Distinct	6	Distinct	1,2,4
Smythii	Sm	−2.0	87.0	840	3	3	2	8	Distinct	6	Distinct	1,2,4
Humorum	Hu	−24.0	320.5	820	3	3	2	8	Distinct	6	Distinct	1,2,4
Apollo	Ap	−36.0	209.0	505	3	3	2	8	Distinct	6	Distinct	1,2,3,4
Moscoviense	Mo	25.0	147.0	445	3	3	2	8	Distinct	6	Distinct	1,2,3,4
Coulomb-Sarton	cs	52.0	237.0	530	3	3	1	7	Distinct	6	Distinct	1,2,3,4
TOP0-30 (Cruger-Sirsalis)[j]	T30	−15.8	293.4	380	3	3	1	7	Distinct	6	Distinct	1,4
Amundsen-Ganswindt	AG	−81.0	120.0	355	3	3	1	7	Distinct	6	Distinct	1,2,4
CTA-25	C25	11.4	350.1	330	3	3	1	7	Distinct	6	Distinct	1
Schiller-Zucchius	SZ	−56.0	315.5	325	3	3	1	7	Distinct	6	Distinct	1,2,4
CTA-10	C10	−25.2	122.3	324	3	3	1	7	Distinct	6	Distinct	1
TOP0-22	T22	50.0	179.8	314	3	3	1	7	Distinct	6	Distinct	1
No name given[k,l]	NN2	−20.0	290.0	300	3	3	1	7	Distinct	6	Distinct	2
Serenitatis	Se	27.0	19.0	740	2	3	3	8	Distinct	5	Distinct	1,2,4
CTA-26	C26	26.5	188.5	533	2	3	3	8	Distinct	5	Distinct	1
Korolev	Ko	−4.5	203.0	440	2	3	3	8	Distinct	5	Distinct	1,2,3,4
TOP0-24 (Dirichlet-Jackson)[j]	T24	13.8	201.7	427	2	3	3	8	Distinct	5	Distinct	1,3
Schrodinger	Sc	−75.0	134.0	320	2	3	3	8	Distinct	5	Distinct	1,2,3,4
TOP0-41	T41	24.8	191.9	317	2	3	3	8	Distinct	5	Distinct	1
Schrodinger-Zeeman[k]	SZe	−81.0	195.0	250	2	3	3	8	Distinct	5	Distinct	2
Imbrium[i]	Im	33.0	342.0	1160	2	3	2	7	Distinct	5	Distinct	1,2,4
TOP0-13	T13	−35.8	148.1	328	2	3	2	7	Distinct	5	Distinct	1
Planck	PI	−57.5	135.5	325	2	3	2	7	Distinct	5	Distinct	1,2,3,4
TOP0-18	T18	−19.2	160.9	805	2	3	1	6	Possible	5	Distinct	1
TOP0-3	T3	55.0	33.7	510	2	3	1	6	Possible	5	Distinct	1
Grimald[i]	Gr	−5.0	292.0	430	2	3	1	6	Possible	5	Distinct	1,2,4
CTA-2	C2	14.2	3.4	419	2	3	1	6	Possible	5	Distinct	1
Lorentz	Lo	34.0	263.0	360	3	2	1	6	Possible	5	Distinct	1,2,3,4
TOP0-15	T15	−64.8	150.3	352	2	3	1	6	Possible	5	Possible	1
Poincaré[i]	Po	−57.5	162.0	340	2	3	1	6	Possible	5	Distinct	1,2,3,4
CTA-23	C23	12.6	306.6	304	2	3	1	6	Possible	5	Distinct	1
Milne[k]	Mi	−31.0	113.0	262	3	1	2	6	Possible	4	Possible	2,4
lnsularum	In	9.0	342.0	600	2	3	0	5	Possible	5	Distinct	1,2,4
CTA-16	C16	50.8	195.5	491	2	3	0	5	Possible	5	Distinct	1
CTA-22	C22	1.8	299.8	401	2	3	0	5	Possible	5	Distinct	1
CTA-17	C17	40.1	210.8	362	2	3	0	5	Possible	5	Distinct	1
CTA-1	C1	1.5	1.2	328	2	3	0	5	Possible	5	Distinct	1
CTA-24	C24	0.4	314.7	323	2	3	0	5	Possible	5	Distinct	1
No name given[k]	NN1	50.0	165.0	450	1	3	3	7	Distinct	4	Possible	2
lngenii[i]	Lg	−34.0	163.0	560	1	3	2	6	Possible	4	Possible	1,2,3,4
Fecunditatis	Fe	−4.0	52.0	990	1	3	1	5	Possible	4	Possible	1,2,4
Tranquillitatis[i]	Tr	7.0	40.0	800	1	3	1	5	Possible	4	Possible	1,2,4
Nubium	Nu	−21.0	345.0	690	1	3	1	5	Possible	4	Possible	1,2,4
TOP0-10	T10	57.8	117.4	603	1	3	1	5	Possible	4	Possible	1
CTA-21	C21	61.9	286.0	468	2	2	1	5	Possible	4	Possible	1
TOP0-1	T1	59.1	2.9	438	1	3	1	5	Possible	4	Possible	1
TOP0-20	T20	39.6	176.4	432	1	3	1	5	Possible	4	Possible	1
CTA-27	C27	18.4	341.6	409	2	2	1	5	Possible	4	Possible	1
TOP0-19	T19	−0.2	170.7	392	1	3	1	5	Possible	4	Possible	1
CTA-7	C7	47.5	95.8	389	1	3	1	5	Possible	4	Possible	1
TOP0-12	T12	−16.3	138.8	329	1	3	1	5	Possible	4	Possible	1
TOP0-9	T9	−50.8	116.7	321	2	2	1	5	Possible	4	Possible	1
Mutus-VIacq	MV	−51.5	21.0	690	1	3	0	4	Possible	4	Possible	1,2,4
Balmer-Kapteyn	BK	−15.5	69.0	550	2	2	0	4	Possible	4	Possible	1,2,4
CTA-19	C19	−34.7	245.8	467	1	3	0	4	Possible	4	Possible	1
No name given[k]	NN3	30.0	165.0	330	1	3	0	4	Possible	4	Possible	2
Mendeleev	Me	6.0	141.0	330	1	2	3	6	Possible	3	Possible	1,2,3,4
Birkhoff	Bi	59.0	213.0	330	1	2	3	6	Possible	3	Possible	1,2,3,4
Bailly	Ba	−67.0	292.0	300	2	1	3	6	Possible	3	Possible	1,2,4
Compton[k]	Co	56.0	104.0	175	0	3	3	6	Possible	3	Possible	2
TOP0-34	T34	−44.0	303.8	317	1	2	2	5	Possible	3	Possible	1
TOP0-32	T32	20.4	297.9	1253	1	2	0	4	Possible	3	Possible	1
TOP0-11	T11	50.1	124.7	824	1	2	1	4	Possible	3	Possible	1
TOP0-17	T17	14.4	156.5	600	1	2	1	4	Possible	3	Possible	1

Table 2. (continued)

Basin Identification[b]					Band-Limited Bouguer Gravity							References[h]
Name	Symbol	Lat (°)	Lon (°)	*D* (km)	gr[c]	*r*[d]	tr[e]	Rating 1[f]		Rating 2[g]		
CTA-6	C6	29.1	80.5	457	1	2	1	4	Possible	3	Possible	1
TOP0-14	T14	−5.5	149.6	446	1	2	1	4	Possible	3	Possible	1
TOP0-2	T2	−15.6	7.0	437	1	2	1	4	Possible	3	Possible	1
CTA-12	C12	−36.8	128.6	360	1	2	1	4	Possible	3	Possible	1
TOP0-33	T33	−38.2	298.0	500	1	2	0	3	Possible	3	Possible	1
CTA-15	C15	−15.3	190.6	490	1	2	0	3	Possible	3	Possible	1
CTA-14	C14	76.6	142.6	744	1	1	1	3	Possible	2	Possible	1
CTA-20	C20	67.8	247.5	501	1	1	1	3	Possible	2	Possible	1
Werner-Airy	WA	−24.0	12.0	500	0	2	1	3	Possible	2	Possible	1,2,4
TOP0-21	T21	−71.6	177.8	377	0	2	1	3	Possible	2	Possible	1
Bailly-Newton[k]	BN	−73.0	303.0	330	1	1	1	3	Possible	2	Possible	2
CTA-13	C13	15.9	135.1	315	1	1	1	3	Possible	2	Possible	1
TOP0-8	T8	−26.9	103.4	314	2	0	1	3	Possible	2	Possible	1
Australe	Au	−51.5	94.5	880	0	2	0	2	Doubtful	2	Possible	1,2,4
Keeler-Heaviside	KH	−10.0	162.0	780	0	2	0	2	Doubtful	2	Possible	1,2,3,4
TOP0-23	T23	−57.1	197.9	696	1	1	0	2	Doubtful	2	Possible	1
Marginis	Ma	20.0	84.0	580	2	0	0	2	Doubtful	2	Possible	1,2,4
Flamsteed-Billy	FB	−7.5	315.0	570	0	2	0	2	Doubtful	2	Possible	1,2,4
TOP0-37	T37	59.2	337.7	470	1	1	0	2	Doubtful	2	Possible	1
CTA-11	C11	27.1	369.0	313	1	1	0	2	Doubtful	2	Possible	1
Sikorsky-Rittenhouse	SR	−68.5	110.0	310	1	1	0	2	Doubtful	2	Possible	1,2,4
Antoniadi[k]	An	−69.0	188.0	140	0	1	3	4	Possible	1	Doubtful	2
TOP0-6	T6	−32.8	87.5	474	0	1	1	2	Doubtful	1	Doubtful	1
TOP0-28	T28	29.6	245.7	392	1	0	1	2	Doubtful	1	Doubtful	1
TOP0-7	T7	−34.2	98.5	389	0	1	1	2	Doubtful	1	Doubtful	1
TOP0-31	T31	42.1	294.4	973	0	1	0	1	Doubtful	1	Doubtful	1
TOP0-4	T4	−46.9	67.0	942	0	1	0	1	Doubtful	1	Doubtful	1
Tsiolkovskiy-Stark	TS	−15.0	128.0	700	0	1	0	1	Doubtful	1	Doubtful	1,2,4
TOP0-25	T25	−57.4	222.7	688	0	1	0	1	Doubtful	1	Doubtful	1
Lomonosov-Fleming	LF	19.0	105.0	620	0	1	0	1	Doubtful	1	Doubtful	1,2,4
AI-Khwarismi King	AK	1.0	112.0	590	0	1	0	1	Doubtful	1	Doubtful	1,2,4
CTA-18	C18	18.6	236.6	539	1	0	0	1	Doubtful	1	Doubtful	1
Sylvester-Nansen[k]	SN	83.0	45.0	500	0	1	0	1	Doubtful	1	Doubtful	2
CTA-3	C3	−24.6	4.3	406	0	1	0	1	Doubtful	1	Doubtful	1
No name given[k]	NN4	45.0	55.0	350	0	1	0	1	Doubtful	1	Doubtful	2
No name given[k]	NN5	60.0	139.0	400	0	1	0	1	Doubtful	1	Doubtful	2
Pingre-Hausen	PH	−56.0	278.0	300	0	1	0	1	Doubtful	1	Doubtful	1,2,4
No name given[k]	NN6	55.0	330.0	700	0	0	1	1	Doubtful	0	Doubtful	2
CTA-4	C4	−83.4	32.9	319	0	0	1	1	Doubtful	0	Doubtful	1
CTA-5	C5	42.3	70.4	309	0	0	1	1	Doubtful	0	Doubtful	1
Grissom-White	GW	−44.0	199.0	600	0	0	0	0	Doubtful	0	Doubtful	1,2,4
CTA-9	C9	23.2	118.2	312	0	0	0	0	Doubtful	0	Doubtful	1
TOP0-40	T40	15.8	347.4	771	–[m]	–[m]	–[m]	–[m]	–[m]	–[m]	–[m]	1
TOP0-16	T16	27.1	150.3	626	–[m]	–[m]	–[m]	–[m]	–[m]	–[m]	–[m]	1
TOP0-38 (inside Imbrium)	T38	37.8	341.2	616	–[m]	–[m]	–[m]	–[m]	–[m]	–[m]	–[m]	1
TOP0-35	T35	−7.7	322.2	451	–[m]	–[m]	–[m]	–[m]	–[m]	–[m]	–[m]	1
TOP0-5	T5	16.6	68.0	428	–[m]	–[m]	–[m]	–[m]	–[m]	–[m]	–[m]	1
TOP0-26	T26	−14.9	240.8	410	–[m]	–[m]	–[m]	–[m]	–[m]	–[m]	–[m]	1
TOP0-27	T27	−10.4	243.8	325	–[m]	–[m]	–[m]	–[m]	–[m]	–[m]	–[m]	1
Procellarum	Pr	26.0	345.0	3200	–[n]	–[n]	–[n]	–[n]	–[n]	–[n]	–[n]	1,2
South Pole-Aitken	SPA	−56.0	180.0	2500	–[n]	–[n]	–[n]	–[n]	–[n]	–[n]	–[n]	1,2,4
CTA-8	C8	19.9	106.8	1764	–[n]	–[n]	–[n]	–[n]	–[n]	–[n]	–[n]	1

[a]The contents are ordered in terms of the basins' ratings from *distinct* to *doubtful*.

[b]Parameters taken from *Frey* [2011, Tables 1–3], if not indicated otherwise. Longitude is given as eastern longitude. Latitude and longitude values have been truncated to one decimal place.

[c]Gravity ring structure: (0) not present; (1) present to some extent; (2) present to a considerable extent; (3) clearly present.

[d]Range (max minus min) over the basin: (0) <50 mGal; (1) 50–100 mGal; (2) 100–150 mGal; (3) >150 mGal.

[e]Topographic rim structure: (0) not visible; (1) visible to some extent; (2) visible to a considerable extent; (3) clearly visible.

[f]Rating 1 (based on the sum of pr, *r*, and tr): (0–2) doubtful; (3–6) possible; (7–9) distinct.

[g]Rating 2 (based on the sum of pr and *r*): (0–1) doubtful; (2–4) possible; (5–6) distinct.

[h]References: 1, *Frey* [2011]; 2, *Wood* [2004]; 3, *Matsumoto et al.* [2010]; 4, *Wieczorek and Le Feuvre* [2009].

[i]Coordinates differ by at least 2 arc degrees to that given by *Frey* [2011]: coordinates given by *Wood* [2004] for Humboldtianum (59.0°N/82.0°E), Imbrium (35.0°N/343.0°E), Poincaré (57.0°S/146.0°E), Ingenii (43.0°S/165.0°E), and Tranqillitatis (7.0°N/30.0°E); coordinates given by *Wieczorek and Le Feuvre* [2009] for Humboldtianum (58.0°N/83.0°E), Imbrium (38.0°N/340.0°E), Poincaré (57.0°S/164.0°E), Ingenii (43.0°S/165.0°E), and Tranqillitatis (7.0°N/30.0°E).

[j]TOP0-24 and TOPO-30 correspond to Dirichlet-Jackson and Cruger-Sirsalis, respectively, as listed by *Wieczorek and Le Feuvre* [2009].

[k]Name and basin identification as provided by *Wood* [2004].

[l]Location corresponds to TOP0-30.

[m]Masked by a strong signal from a nearby basin.

[n]Not present in the band-limited Bouguer gravity as long spatial scales have been removed.

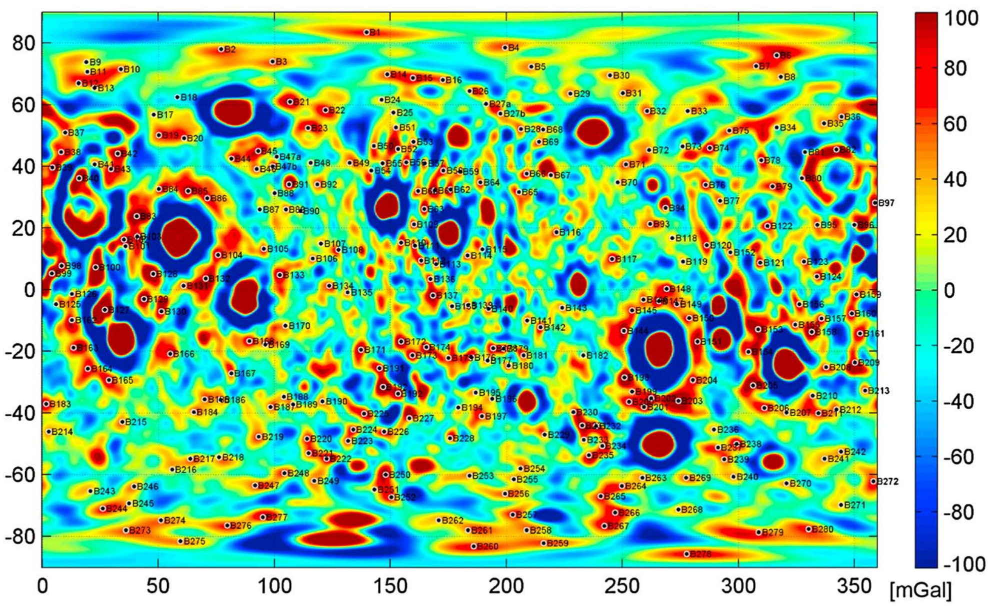

Figure 6. Spatial distribution of all newly identified locations of band-limited Bouguer gravity signatures. The spectral band is $n1 = 18$ to $n2 = 70$, corresponding to spatial scales between ~300 km and ~80 km and a limiting depth of ~100 km. The locations, full names, and descriptions are given in Appendix A. Rectangular projection.

presence of Fitzgerald-Jackson (named TOPO-41 in *Frey* [2011, p. 57]) from analysis of farside lunar topography only. Also, based only on topographic data, *Frey* [2011] postulated a likely basin to the east of Debye (named TOPO-22 in *Frey* [2011, p. 57]). We believe that the anomalous mass feature identified in our study at 50°N, 180°E is the corresponding gravity field signature, thus providing further evidence for both being real basins.

[24] Figure 3 shows zoomed-in plots of the full-resolution LOLA topography and the band-limited (degrees $n1 = 18$ to $n2 = 70$) Bouguer gravity for the three basins considered here. For Hertzsprung, the presence of the basin is evident in both the topography (Figure 3a) and the band-limited gravity (Figure 3b). The band-limited gravity exhibits a circular central gravity high surrounded by a negative gravity annulus (circular gravity high-low) that is correlated spatially with the topographic signature. As this is a well-established basin, this shows that the band-limited technique is capable of detecting basins.

[25] For Fitzgerald-Jackson, Figure 3c shows that the basin is not as clearly defined by the LOLA topography alone. However, Figure 3d shows a mass anomaly that correlates spatially with a broad topographic low. There is less evidence of a circular gravity high-low structure that was so clear for Hertzsprung. As stated, *Huang et al*. [2009] and *Frey* [2011] did not use gravity data to identify this basin. However, when both data sets are considered together, we believe that they provide stronger evidence of the presence of a real basin.

[26] The basin near Debye is hardly discernible from the LOLA topography alone (Figure 3e), with masking caused by the many smaller-scale basins scattered throughout this region. On the other hand, a mass anomaly is clearer from the band-limited gravity, which also shows a circular gravity high-low signature. Given that the band-limited technique has proven effective over Hertzsprung and Fitzgerald-Jackson, we infer that it has correctly identified this as a basin.

3.1. Sensitivity Analyses

[27] The lunar maps presented in Figures 1–3 use a constant topographic mass density for the topography-implied gravity of 2700 kg m^{-3} as the mean of pre-GRAIL mass densities over many farside regions [*Huang and Wieczorek*, 2012]. We therefore conducted a sensitivity analysis based on the end-members of more recently published lunar topographic mass densities [*Wieczorek et al*., 2013; *Huang and Wieczorek*, 2012; *Kiefer et al*., 2012]. Figure 4 shows that the topographic mass density between the end-members of 2400 kg m^{-3} to 2900 kg m^{-3} makes no difference to the spatial mapping of these three basins; each is mapped to exactly the same location irrespective of the mass density chosen. One minor exception is that the lower density estimate more clearly identifies the annular gravity low around Hertzsprung (Figure 4a).

[28] We also conducted sensitivity analyses to the degree of band limiting. Table 1 shows the spatial scales resolved (equation (6)) and the limiting depths according to Bowin's relation (equation (5)). These bands have been chosen somewhat arbitrarily but only to show the effect of the bandwidth on the identification of the basins. Figure 5 shows that the higher the starting degree $n1$ of the summations in equations (1) and (4), the lower the amplitude of the signature of the basins, thus lessening the method's resolving power. This is particularly the case for Fitzgerald-Jackson, so caution needs to be exercised for higher degrees of filtering. Nevertheless, the identification of the basins remains quite robust for the lower range of degrees of filtering.

4. Classification of Lunar Basin Locations

[29] We next use band-limited Bouguer gravity and topography to perform a classification of previously reported lunar basins as listed or postulated by *Wood* [2004], *Frey* [2011], *Wieczorek and Le Feuvre* [2009], and *Matsumoto et al*. [2010]. Based on the sensitivity analyses (section 3.1), we use the band-limited Bouguer gravity ($n1 = 18$ to $n2 = 70$)

Table 3. Identification of New Locations of Significant Band-Limited Bouguer Gravity Signals That Are Classified as *Distinct* in One or Both of Ratings 1 and 2 (See Appendix A for a Complete List)

Basin Identification[a]					Band-Limited Bouguer Gravity							
Name	Symbol	Lat (°)	Lon (°)	*D* (km)	gr[b]	*r*[c]	tr[d]	Rating 1[e]		Rating 2[f]		Comments[g]
BBG-67	B67	37.2	219.1	320	3	3	3nc	9	Distinct	6	Distinct	Part of cluster 15 south of CTA-17
BBG-91	B91	34.2	106.3	180	3	3	3c	9	Distinct	6	Distinct	Between clusters 12 and 20
BBG-128	B128	5.2	47.7	460	3	3	2c	8	Distinct	6	Distinct	Between Tr and Fe
BBG-228	B228	−48.1	175.6	220	3	3	2c	8	Distinct	6	Distinct	
BBG-66	B66	37.7	208.6	180	3	3	2c	8	Distinct	6	Distinct	Part of cluster 15 south of CTA-17
BBG-52	B52	45.6	153.2	240	2	3	3c	8	Distinct	5	Distinct	Part of cluster 13 north of Mo
BBG-47a	B47a	43.2	100.9	200	3	2	3nc	8	Distinct	5	Distinct	Part of cluster 12 south of CTA-7
BBG-100	B100	7.4	22.9	460	3	3	1c	7	Distinct	6	Distinct	Within impact basin of Tr
BBG-96	B96	21.0	350.0	400	3	3	1nc	7	Distinct	6	Distinct	Part of cluster 21; close to Pr, CTA-27, and TOPO-40
BBG-127	B127	−6.5	26.9	420	3	3	1c	7	Distinct	6	Distinct	Located partly within impact basin of Ne
BBG-117	B117	10.0	245.5	320	3	3	1c	7	Distinct	6	Distinct	
BBG-94	B94	26.5	268.5	300	3	3	1c	7	Distinct	6	Distinct	South of Lo
BBG-209	B209	−23.7	350.1	400	2	3	2c	7	Distinct	5	Distinct	Southeast of Nu
BBG-198	B198	−28.4	250.9	280	2	3	2c	7	Distinct	5	Distinct	Part of cluster 38 between Or and CTA-19
BBG-23	B23	52.4	114.5	260	2	3	2c	7	Distinct	5	Distinct	Part of cluster 6 around TOPO-10
BBG-73	B73	46.5	275.8	260	2	3	2nc	7	Distinct	5	Distinct	Part of cluster 18
BBG-40	B40	36.1	15.8	260	2	3	2c	7	Distinct	5	Distinct	Within the impact basin of Se
BBG-213	B213	−32.7	354.5	260	3	2	2c	7	Distinct	5	Distinct	
BBG-227	B227	−41.6	158.2	260	2	3	2nc	7	Distinct	5	Distinct	Southwest of In
BBG-6	B6	76.0	316.4	220	2	3	2c	7	Distinct	5	Distinct	Part of cluster 2
BBG-21	B21	61.0	106.8	200	2	3	2c	7	Distinct	5	Distinct	Part of cluster 6 around TOPO-10
BBG-277	B277	−73.7	95.0	160	2	3	2c	7	Distinct	5	Distinct	Part of cluster 53 southwest of SR
BBG-278	B278	−85.6	277.7	100	3	2	2c	7	Distinct	5	Distinct	
BBG-81	B81	44.6	328.6	280	1	3	3nc	7	Distinct	4	Possible	Partly within impact basin of Im
BBG-47b	B47b	39.9	99.1	280	2	2	3c	7	Distinct	4	Possible	Part of cluster 12 south of CTA-7
BBG-32	B32	57.9	260.5	220	2	2	3nc	7	Distinct	4	Possible	Part of cluster 8
BBG-115	B115	13.2	189.6	220	2	2	3nc	7	Distinct	4	Possible	Part of cluster 26 southeast of FS
BBG-118	B118	16.9	271.5	200	2	2	3c	7	Distinct	4	Possible	
BBG-27b	B27b	57.1	197.5	180	2	2	3nc	7	Distinct	4	Possible	Part of cluster 7; between Bi and CTA-16
BBG-54	B54	38.6	141.8	140	2	2	3nc	7	Distinct	4	Possible	Part of cluster 13 north of Mo
BBG-83	B83	23.8	40.7	360	2	3	1c	6	Possible	5	Distinct	Between Se and Cr
BBG-163	B163	−18.8	13.4	360	2	3	1c	6	Possible	5	Distinct	Between Ne, WA, and TOPO-2
BBG-162	B162	−9.9	12.8	320	2	3	1c	6	Possible	5	Distinct	Between Ne, WA, and TOPO-2
BBG-113	B113	8.3	169.7	200	3	2	1c	6	Possible	5	Distinct	
BBG-43	B43	39.2	29.7	160	2	3	1c	6	Possible	5	Distinct	Part of cluster 11
BBG-26	B26	64.4	184.0	120	3	2	1nc	6	Possible	5	Distinct	Part of cluster 7
BBG-203	B203	−36.0	274.0	400	2	3	0	5	Possible	5	Distinct	Between Or and MR
BBG-158	B158	−13.7	331.6	360	2	3	0	5	Possible	5	Distinct	Part of cluster 30 around TOPO-30, north of Hu
BBG-205	B205	−30.9	306.2	360	2	3	0	5	Possible	5	Distinct	Southwest of Hu
BBG-129	B129	−3.0	43.7	340	2	3	0	5	Possible	5	Distinct	Part of cluster 28 around Fe
BBG-137	B137	−1.8	168.4	320	2	3	0	5	Possible	5	Distinct	Part of cluster 29 around TOPO-19
BBG-161	B161	−14.2	352.4	320	2	3	0	5	Possible	5	Distinct	Part of cluster 31; northeast of Nu
BBG-130	B130	−7.0	51.4	300	2	3	0	5	Possible	5	Distinct	Part of cluster 28 around Fe
BBG-172	B172	−16.9	154.7	300	2	3	0	5	Possible	5	Distinct	Part of cluster 33, band including TOPO-18
BBG-97	B97	28.2	358.8	280	2	3	0	5	Possible	5	Distinct	Part of cluster 21; joins cluster 10
BBG-173	B173	−21.3	159.6	280	2	3	0	5	Possible	5	Distinct	Part of cluster 33, band including TOPO-18
BBG-42	B42	44.2	32.5	260	2	3	0	5	Possible	5	Distinct	Part of cluster 11
BBG-174	B174	−18.7	165.4	260	2	3	0	5	Possible	5	Distinct	Part of cluster 33, band including TOPO-18
BBG-165	B165	−29.3	28.6	260	2	3	0	5	Possible	5	Distinct	Between Ne and WA
BBG-192	B192	−31.4	146.8	260	2	3	0	5	Possible	5	Distinct	Part of cluster 36, north of TOPO-13
BBG-22	B22	58.2	122.1	240	2	3	0	5	Possible	5	Distinct	Part of cluster 6 around TOPO-10
BBG-122	B122	20.7	312.5	240	2	3	0	5	Possible	5	Distinct	
BBG-168	B168	−16.6	89.3	240	2	3	0	5	Possible	5	Distinct	Part of cluster 32 south of Sm
BBG-171	B171	−19.4	137.3	240	2	3	0	5	Possible	5	Distinct	South of TOPO-12
BBG-109	B109	21.2	160.1	220	2	3	0	5	Possible	5	Distinct	Between Mo and FS
BBG-191	B191	−25.4	145.3	220	2	3	0	5	Possible	5	Distinct	Part of cluster 36
BBG-183	B183	−37.0	1.7	220	2	3	0	5	Possible	5	Distinct	
BBG-74	B74	46.0	287.6	200	2	3	0	5	Possible	5	Distinct	Part of cluster 18
BBG-121	B121	8.8	309.4	200	2	3	0	5	Possible	5	Distinct	South of CTA-23
BBG-193	B193	−33.6	153.2	200	2	3	0	5	Possible	5	Distinct	Part of cluster 36, north of TOPO-13
BBG-63	B63	26.2	164.7	180	2	3	0	5	Possible	5	Distinct	Part of cluster 14 between Mo and TOPO-20
BBG-101	B101	14.1	30.3	180	2	3	0	5	Possible	5	Distinct	Part of cluster 23; between Se and Cr
BBG-238	B238	−50.0	299.2	180	2	3	0	5	Possible	5	Distinct	Part of cluster 44 between MR and SZ
BBG-112	B112	9.5	163.2	160	2	3	0	5	Possible	5	Distinct	Part of cluster 25 around TOPO-17
BBG-236	B236	−45.3	289.4	160	3	2	0	5	Possible	5	Distinct	Part of cluster 44 between MR and SZ
BBG-56	B56	41.3	156.9	140	2	3	0	5	Possible	5	Distinct	Part of cluster 13 north of Mo

[a]Name reflects band-limited Bouguer gravity (BGG). Longitude is given as eastern longitude. Rim diameter *D* is approximated to the nearest 20 km and is based on the spatial extent of the topographic signature or on the gravity signature in case no topographic signature is present (e.g., tr = 0).

and a topographic mass density of 2700 kg m^{-3}, corresponding to spatial scales (half wavelength) of ~300 km down to ~80 km. This is now applied over the entire lunar surface.

[30] The classification is based on three indicators: (i) the presence of a circular gravity high-low structure in the band-limited Bouguer gravity, (ii) the range (maximum minus minimum) of band-limited Bouguer gravity over the supposed basin, and (iii) the presence of a topographic rim structure. We interpret a circular gravity high-low structure in the band-limited Bouguer gravity as an indication of a regional mass density anomaly that largely follows the same spatial pattern. A large range indicates a significant mass density anomaly. The third indicator is included because most already known basins also show a topographic signature [cf. *Frey*, 2011].

[31] Each indicator is assigned four somewhat subjectively determined numerical values: (0) not seemingly present, (1) present to some limited extent, (2) present to some considerable extent, and (3) quite clearly present. From these three indicators, two ratings are derived: Rating 1 is based on the sum of all indicators, including the topographic signatures (i, ii, and iii); Rating 2 is based on the sum of only the two band-limited Bouguer gravity-related indicators (i and ii). Similar to the approach of *Frey* [2011], each rating is then assigned to one of three classes in order to classify the supposed basin locations: *doubtful*, *possible*, and *distinct*.

[32] Most of the 122 known or postulated basins listed in Table 2, including our three case study basins (section 3), are classified as either *distinct* or *possible*. Our classification supports the presence of several basins proposed by *Frey* [2011] that exhibit anomalous thin crustal thickness but no topographic signature (classified here as *distinct* or *possible*). Table 2 also lists several basins postulated by *Frey* [2011] based on their topographic signature only, but which do not exhibit a clear signature in the band-limited Bouguer gravity and are thus classified as *doubtful*.

[33] Using the band-limited Bouguer gravity, we identify positive signals with a classification of *possible* or *distinct* and a minimum resolvable spatial scale of ~80 km. These have (i) a circular gravity high-low structure to some extent, (ii) a range of >50 mGal, and (iii) a topographic rim structure to some extent. If no part of a topographic rim structure is evident, only the strong gravity signals with a range of >100 mGal are included. From all the so-identified signals, we exclude those that are centered over the basin locations listed in Table 2 but do retain signals that are close to them. This resulted in a total of 280 band-limited Bouguer gravity signals that indicate locations of significant mass density surpluses (Figure 6 and Appendix A). Table 3 lists only the 66 locations that are classified as *distinct* by at least one of the two above ratings; the remainder is listed in Appendix A.

[34] Of the 280 band-limited Bouguer gravity signals examined, 174 are colocated with a complete or part of a topographic rim structure, providing some more confidence that they are indeed basins. The locations and diameters *D* listed in Table 3 and Appendix A are based on either the topographic rim, if present, or the location and spatial extent of the band-limited Bouguer gravity signal. The extracted diameters range from ~100 km to ~760 km with the majority (246 of 280) less than ~300 km, slightly larger than the resolving power of the band-limited Bouguer gravity (~80 km). Many of the basins classified in Table 3 and Appendix A are close to or partly located within existing basins or form part of a cluster of basins. These weaker signals are only revealed when using band-limited Bouguer gravity but obscured when using full-banded Bouguer gravity.

5. Summary and Conclusions

[35] Three case studies over the farside of the Moon have demonstrated the ability of *band-limited* Bouguer gravity to identify and map lunar basins that are not detected so clearly with full-spectrum Bouguer gravity or topography alone [cf. *Huang et al*., 2009; *Namiki et al*., 2009; *Matsumoto et al*., 2010; *Frey*, 2011]. The band-limited Bouguer gravity enhances the signatures of small-scale structures by suppressing long wavelengths that can hamper localized investigations. This has revealed signatures of two distinct mass concentrations on the lunar farside. The Fitzgerald-Jackson (25°N, 191°E) gravity signature is also partly visible as a topographic feature but can now be better classified as a basin with inner mass excess. The gravity signature to the east of Debye (50° N, 180°E) lacks an obvious corresponding topographic signature, albeit identified by *Frey* [2011] as a candidate basin. The band-limited gravity signature adds evidence that this is indeed a real basin. The positive band-limited gravity signatures at their centers indicate mass excesses with respect to their surrounds, which could reflect mantle uplift postimpact [cf. *Neumann et al*., 1996; *Wieczorek et al*., 2006].

[36] After showing the band-limited approach to be a robust tool for identifying candidate basins on the more challenging farside for some selected bandwidths and end-members of the likely lunar topographic mass density, we have applied it over the entire lunar surface. This was done for spectral bands $n1 = 18$ to $n2 = 70$, corresponding to spatial scales between ~300 km and ~80 km and a limiting depth of ~100 km. A combination of indicators, including the topography-only signature, was used to determine whether the candidate basin was *distinct* or *possible*. Of the 280 candidate basins, 66 have been classified as distinct. We have deliberately restricted this study to the identification and mapping of the basins rather than attempting an interpretation of their origins and relation to lunar history; this is left for future work.

6. Note Added During Review

[37] The embryonic part of this work was carried out and submitted before results from the GRAIL mission became available in December 2012. We submitted a first version back

[b]Gravity ring structure: (0) not present; (1) present to some extent; (2) present to considerable extent; (3) clearly present.
[c]Range (max minus min) over the basin: (0) <50 mGal; (1) 50–100 mGal; (2) 100–150 mGal; (3) >150 mGal.
[d]Topographic rim structure: (0) not visible; (1) visible to some extent; (2) visible to a considerable extent; (3) clearly visible. The letter c indicates that the gravity ring structure is centred over the topographic rim structure, while the letters nc indicate that it is not centred.
[e]Rating 1 (based on the sum of pr, *r*, and tr): (0–2) doubtful; (3–6) possible; (7–9) distinct.
[f]Rating 2 (based on the sum of pr and *r*): (0–1) doubtful; (2–4) possible; (5–6) distinct.
[g]Cluster indicates multiple impacts with partly overlapping gravity and topography signals. Reference to existing impact basins indicates their closeness to the identified signal; names and abbreviations used refer to those in Table 2.

in October 2011 and a revision in November 2012, both describing band-limited Bouguer gravity for improved mapping of lunar gravity signatures and substantiating the two farside basins. Preliminary results or papers from the GRAIL mission were thus not available to us to draft our manuscript. Only after the release of preliminary GRAIL results, we were able to incorporate different topographic mass density estimates in section 3, but which did not alter our conclusions. The GRAIL Bouguer gravity map published by *Zuber et al.* [2013, Figure 1B] shows signatures of 100 mGal (or more) in amplitude at 25°N, 191°E and 50°N, 180°E, hence providing post facto independent evidence of the basins.

Appendix A: Full List of Band-Limited Bouguer Gravity Basins

This appendix provides a list of all new 280 locations of band-limited Bouguer gravity signals that are classified as either distinct or possible (Table A1).

Table A1. Identification of All New Locations of Band-Limited Bouguer Gravity Signals That Are Classified as Either *Distinct* or *Possible* in Ratings 1 and 2

Basin Identification[a]					Band-Limited Bouguer Gravity							
Name	Symbol	Lat (°)	Lon (°)	*D* (km)	gr[b]	*r*[c]	tr[d]	Rating 1[e]		Rating 2[f]		Comments[g]
BBG-1	B1	83.5	139.7	180	2	2	0	4	Possible	4	Possible	
BBG-2	B2	77.9	77.1	160	2	2	2c	6	Possible	4	Possible	Cluster 1
BBG-3	B3	74.0	99.3	140	1	2	1c	4	Possible	3	Possible	Cluster 1
BBG-4	B4	78.4	199.4	160	2	2	1c	5	Possible	4	Possible	
BBG-5	B5	72.2	210.7	140	2	2	1c	5	Possible	4	Possible	
BBG-6	B6	76.0	316.4	220	2	3	2c	7	Distinct	5	Distinct	Cluster 2
BBG-7	B7	72.5	307.5	260	1	2	2c	5	Possible	3	Possible	Cluster 2
BBG-8	B8	69.0	318.3	160	1	2	2c	5	Possible	3	Possible	Cluster 2
BBG-9	B9	73.7	18.9	140	1	2	2nc	5	Possible	3	Possible	Cluster 3
BBG-10	B10	71.5	33.7	140	1	2	1c	4	Possible	3	Possible	Cluster 3
BBG-11	B11	70.6	19.3	80	1	2	2nc	5	Possible	3	Possible	Cluster 3
BBG-12	B12	66.9	15.7	160	1	2	1nc	4	Possible	3	Possible	Cluster 3
BBG-13	B13	65.4	22.6	140	1	2	1nc	4	Possible	3	Possible	Cluster 3
BBG-14	B14	69.8	148.6	140	1	2	1c	4	Possible	3	Possible	Cluster 4
BBG-15	B15	68.6	159.8	160	1	3	2c	6	Possible	4	Possible	Cluster 4
BBG-16	B16	68.0	172.5	120	1	2	1c	4	Possible	3	Possible	Cluster 4
BBG-17	B17	56.8	46.5	140	1	1	1c	3	Possible	2	Possible	Cluster 5 north of NN4
BBG-18	B18	56.0	58.3	120	1	2	3nc	6	Possible	3	Possible	Cluster 5 north of NN4
BBG-19	B19	50.2	50.2	160	1	2	1c	4	Possible	3	Possible	Cluster 5 north of NN4
BBG-20	B20	49.2	61.0	180	1	2	2c	5	Possible	3	Possible	Cluster 5 north of NN4
BBG-21	B21	61.0	106.8	200	2	3	2c	7	Distinct	5	Distinct	Cluster 6 around TOPO-10
BBG-22	B22	58.2	122.1	240	2	3	0	5	Possible	5	Distinct	Cluster 6 around TOPO-10
BBG-23	B23	52.4	114.5	260	2	3	2c	7	Distinct	5	Distinct	Cluster 6 around TOPO-10
BBG-24	B24	61.6	146.1	140	1	1	3c	5	Possible	2	Possible	Close to NN5
BBG-25	B25	57.4	151.3	140	1	1	1c	3	Possible	2	Possible	
BBG-26	B26	64.4	184.0	120	3	2	1nc	6	Possible	5	Distinct	Cluster 7
BBG-27a	B27a	60.2	191.3	160	2	2	2nc	6	Possible	4	Possible	Cluster 7
BBG-27b	B27b	57.1	197.5	180	2	2	3nc	7	Distinct	4	Possible	Cluster 7; between Bi and CTA-16
BBG-28	B28	52.2	206.3	160	2	2	0	4	Possible	4	Possible	Cluster 7; between Bi and CTA-16
BBG-29	B29	63.6	227.6	120	2	2	1c	5	Possible	4	Possible	
BBG-30	B30	69.5	244.7	140	2	2	0	4	Possible	4	Possible	Cluster 8
BBG-31	B31	63.8	250.1	160	1	2	1c	4	Possible	3	Possible	Cluster 8
BBG-32	B32	57.9	260.5	220	2	2	3nc	7	Distinct	4	Possible	Cluster 8
BBG-33	B33	57.9	278.2	140	1	2	3nc	6	Possible	3	Possible	
BBG-34	B34	52.6	316.5	340	1	3	2nc	6	Possible	4	Possible	Joins with BBG-75 of cluster 18
BBG-35	B35	54.0	336.8	180	1	2	1c	4	Possible	3	Possible	Cluster 9; south of TOPO-37
BBG-36	B36	56.1	344.3	140	1	2	1c	4	Possible	3	Possible	Cluster 9; south of TOPO-37
BBG-37	B37	51.0	9.8	200	1	2	1nc	4	Possible	3	Possible	Cluster 10 connected to TOPO-1
BBG-38	B38	44.7	8.1	260	1	2	2c	5	Possible	3	Possible	Cluster 10 connected to TOPO-1
BBG-39	B39	39.6	4.3	220	1	3	1c	5	Possible	4	Possible	Cluster 10 connected to TOPO-1
BBG-40	B40	36.1	15.8	260	2	3	2c	7	Distinct	5	Distinct	Within the impact basin of Se
BBG-41	B41	40.7	22.6	160	2	2	1c	5	Possible	4	Possible	Cluster 11
BBG-42	B42	44.2	32.5	260	2	3	0	5	Possible	5	Distinct	Cluster 11
BBG-43	B43	39.2	29.7	160	2	3	1c	6	Possible	5	Distinct	Cluster 11
BBG-44	B44	42.5	81.5	180	1	3	2c	6	Possible	4	Possible	Cluster 12 south of CTA-7
BBG-45	B45	45.0	92.9	240	1	3	0	4	Possible	4	Possible	Cluster 12 south of CTA-7
BBG-46	B46	39.2	92.3	180	2	2	0	4	Possible	4	Possible	Cluster 12 south of CTA-7
BBG-47a	B47a	43.2	100.9	200	3	2	3nc	8	Distinct	5	Distinct	Cluster 12 south of CTA-7
BBG-47b	B47b	39.9	99.1	280	2	2	3c	7	Distinct	4	Possible	Cluster 12 south of CTA-7
BBG-48	B48	41.1	115.6	160	2	1	2c	5	Possible	3	Possible	
BBG-49	B49	41.1	132.5	200	1	2	1c	4	Possible	3	Possible	Cluster 13 north of Mo
BBG-50	B50	46.6	142.9	160	1	2	2nc	5	Possible	3	Possible	Cluster 13 north of Mo
BBG-51	B51	52.7	152.5	120	1	2	1c	4	Possible	3	Possible	Cluster 13 north of Mo
BBG-52	B52	45.6	153.2	240	2	3	3c	8	Distinct	5	Distinct	Cluster 13 north of Mo

Table A1. (continued)

Basin Identification[a]					Band-Limited Bouguer Gravity							
Name	Symbol	Lat (°)	Lon (°)	*D* (km)	gr[b]	*r*[c]	tr[d]	Rating 1[e]		Rating 2[f]		Comments[g]
BBG-53	B53	47.9	160.0	140	1	2	0	3	Possible	3	Possible	Cluster 13 north of Mo
BBG-54	B54	38.6	141.8	140	2	2	3nc	7	Distinct	4	Possible	Cluster 13 north of Mo
BBG-55	B55	41.0	146.6	120	1	2	3nc	6	Possible	3	Possible	Cluster 13 north of Mo
BBG-56	B56	41.3	156.9	140	2	3	0	5	Possible	5	Distinct	Cluster 13 north of Mo
BBG-57	B57	41.0	164.9	140	2	2	0	4	Possible	4	Possible	Cluster 14 between Mo and TOPO-20
BBG-58	B58	38.7	172.8	180	1	3	0	4	Possible	4	Possible	Cluster 14 between Mo and TOPO-20
BBG-59	B59	38.3	179.8	140	1	2	0	3	Possible	3	Possible	Cluster 14 between Mo and TOPO-20
BBG-60	B60	32.0	161.9	180	2	2	0	4	Possible	4	Possible	Cluster 14 between Mo and TOPO-20
BBG-61	B61	32.1	169.0	220	1	3	0	4	Possible	4	Possible	Cluster 14 between Mo and TOPO-20
BBG-62	B62	32.4	175.9	200	1	3	0	4	Possible	4	Possible	Cluster 14 between Mo and TOPO-20
BBG-63	B63	26.2	164.7	180	2	3	0	5	Possible	5	Distinct	Cluster 14 between Mo and TOPO-20
BBG-64	B64	34.8	188.7	160	2	2	0	4	Possible	4	Possible	Cluster 14 between Mo and TOPO-20
BBG-65	B65	31.6	205.3	220	1	2	1c	4	Possible	3	Possible	
BBG-66	B66	37.7	208.6	180	3	3	2c	8	Distinct	6	Distinct	Cluster 15 south of CTA-17
BBG-67	B67	37.2	219.1	320	3	3	3nc	9	Distinct	6	Distinct	Cluster 15 south of CTA-17
BBG-68	B68	52.0	215.8	120	1	2	3c	6	Possible	3	Possible	Cluster 16 between Bi and CTA-17
BBG-69	B69	47.9	214.0	160	2	2	0	4	Possible	4	Possible	Cluster 16 between Bi and CTA-17
BBG-70	B70	34.8	248.0	200	2	2	1c	5	Possible	4	Possible	Cluster 17 between CS and Lo
BBG-71	B71	40.6	251.5	220	1	2	2c	5	Possible	3	Possible	Cluster 17 between CS and Lo
BBG-72	B72	45.3	261.5	220	1	2	2nc	5	Possible	3	Possible	Cluster 17 between CS and Lo
BBG-73	B73	46.5	275.8	260	2	3	2nc	7	Distinct	5	Distinct	Cluster 18
BBG-74	B74	46.0	287.6	200	2	3	0	5	Possible	5	Distinct	Cluster 18
BBG-75	B75	51.6	296.1	180	1	2	0	3	Possible	3	Possible	Cluster 18; joins with BBG-34
BBG-76	B76	33.9	285.8	180	1	3	0	4	Possible	4	Possible	Cluster 19
BBG-77	B77	28.8	292.1	180	1	2	0	3	Possible	3	Possible	Cluster 19
BBG-78	B78	41.9	309.7	200	1	3	1c	5	Possible	4	Possible	
BBG-79	B79	33.4	314.7	440	1	2	1c	4	Possible	3	Possible	
BBG-80	B80	36.1	327.4	360	1	3	1nc	5	Possible	4	Possible	Partly within impact basin of Im
BBG-81	B81	44.6	328.6	280	1	3	3nc	7	Distinct	4	Possible	Partly within impact basin of Im
BBG-82	B82	45.4	342.1	400	1	3	1c	5	Possible	4	Possible	Partly within impact basin of Im
BBG-83	B83	23.8	40.7	360	2	3	1c	6	Possible	5	Distinct	Between Se and Cr
BBG-84	B84	32.7	50.2	260	1	3	1c	5	Possible	4	Possible	North of Cr
BBG-85	B85	31.9	62.8	280	1	3	1c	5	Possible	4	Possible	North of Cr
BBG-86	B86	29.7	71.1	240	1	3	0	4	Possible	4	Possible	North of Cr
BBG-87	B87	25.9	93.6	180	2	1	3nc	6	Possible	3	Possible	Cluster 20; north of LF
BBG-88	B88	31.3	100.0	180	1	1	3c	5	Possible	2	Possible	Cluster 20; north of LF
BBG-89	B89	26.0	104.9	240	1	2	1c	4	Possible	3	Possible	Cluster 20; north of LF
BBG-90	B90	25.5	111.1	200	1	1	1c	3	Possible	2	Possible	Cluster 20; north of LF
BBG-91	B91	34.2	106.3	180	3	3	3c	9	Distinct	6	Distinct	Between clusters 12 and 20
BBG-92	B92	34.2	118.5	200	2	2	2c	6	Possible	4	Possible	
BBG-93	B93	21.3	261.9	280	1	2	1c	4	Possible	3	Possible	
BBG-94	B94	26.5	268.5	300	3	3	1c	7	Distinct	6	Distinct	South of Lo
BBG-95	B95	21.0	333.9	260	1	3	0	4	Possible	4	Possible	West of CTA-27
BBG-96	B96	21.0	350.0	400	3	3	1nc	7	Distinct	6	Distinct	Cluster 21; close to Pr, CTA-27, and TOPO-40
BBG-97	B97	28.2	358.8	280	2	3	0	5	Possible	5	Distinct	Cluster 21; joins cluster 10
BBG-98	B98	7.9	8.3	240	1	3	0	4	Possible	4	Possible	Cluster 22; between CTA-1 and CTA-2
BBG-99	B99	5.3	4.1	260	1	3	0	4	Possible	4	Possible	Cluster 22; between CTA-1 and CTA-2
BBG-100	B100	7.4	22.9	460	3	3	1c	7	Distinct	6	Distinct	Within impact basin of Tr
BBG-101	B101	14.1	30.3	180	2	3	0	5	Possible	5	Distinct	Cluster 23; between Se and Cr
BBG-102	B102	16.3	35.2	220	1	3	0	4	Possible	4	Possible	Cluster 23; between Se and Cr
BBG-103	B103	17.3	40.8	220	1	3	0	4	Possible	4	Possible	Cluster 23; between Se and Cr
BBG-104	B104	11.4	75.8	260	1	3	0	4	Possible	4	Possible	Between Cr and Sm
BBG-105	B105	13.4	95.5	220	2	2	0	4	Possible	4	Possible	
BBG-106	B106	10.1	116.5	240	2	2	0	4	Possible	4	Possible	Cluster 24
BBG-107	B107	15.0	120.0	240	2	2	2c	6	Possible	4	Possible	Cluster 24
BBG-108	B108	13.0	127.6	240	1	2	1c	4	Possible	3	Possible	Cluster 24
BBG-109	B109	21.2	160.1	220	2	3	0	5	Possible	5	Distinct	Between Mo and FS
BBG-110	B110	15.3	154.6	160	1	3	0	4	Possible	4	Possible	Cluster 25 around TOPO-17
BBG-111	B111	14.4	160.6	160	1	3	0	4	Possible	4	Possible	Cluster 25 around TOPO-17
BBG-112	B112	9.5	163.2	160	2	3	0	5	Possible	5	Distinct	Cluster 25 around TOPO-17
BBG-113	B113	8.3	169.7	200	3	2	1c	6	Possible	5	Distinct	
BBG-114	B114	11.2	183.2	200	2	2	0	4	Possible	4	Possible	Cluster 26 southeast of FS
BBG-115	B115	13.2	189.6	220	2	2	3nc	7	Distinct	4	Possible	Cluster 26 southeast of FS
BBG-116	B116	18.7	221.5	200	2	2	0	4	Possible	4	Possible	Part of a cluster east of TOPO-24
BBG-117	B117	10.0	245.5	320	3	3	1c	7	Distinct	6	Distinct	
BBG-118	B118	16.9	271.5	200	2	2	3c	7	Distinct	4	Possible	
BBG-119	B119	9.2	276.0	260	2	2	1c	5	Possible	4	Possible	
BBG-120	B120	14.5	286.3	240	1	2	0	3	Possible	3	Possible	
BBG-121	B121	8.8	309.4	200	2	3	0	5	Possible	5	Distinct	South of CTA-23

Table A1. (continued)

Basin Identification[a]					Band-Limited Bouguer Gravity							
Name	Symbol	Lat (°)	Lon (°)	D (km)	gr[b]	r[c]	tr[d]	Rating 1[e]		Rating 2[f]		Comments[g]
BBG-122	B122	20.7	312.5	240	2	3	0	5	Possible	5	Distinct	
BBG-123	B123	9.1	328.1	260	1	2	1c	4	Possible	3	Possible	Cluster 27 west of In
BBG-124	B124	4.3	333.8	260	2	2	1c	5	Possible	4	Possible	Cluster 27 west of In
BBG-125	B125	−4.7	5.9	280	1	2	1nc	4	Possible	3	Possible	Southwest of CTA-1
BBG-126	B126	−1.4	12.8	280	1	2	1c	4	Possible	3	Possible	Southwest of CTA-1
BBG-127	B127	−6.5	26.9	420	3	3	1c	7	Distinct	6	Distinct	Located partly within impact basin of Ne
BBG-128	B128	5.2	47.7	460	3	3	2c	8	Distinct	6	Distinct	Between Tr and Fe
BBG-129	B129	−3.0	43.7	340	2	3	0	5	Possible	5	Distinct	Cluster 28 around Fe
BBG-130	B130	−7.0	51.4	300	2	3	0	5	Possible	5	Distinct	Cluster 28 around Fe
BBG-131	B131	1.4	60.8	240	1	2	1c	4	Possible	3	Possible	Northeast of Fe
BBG-132	B132	3.6	70.3	420	1	3	1c	5	Possible	4	Possible	Between Cr and Sm
BBG-133	B133	4.8	102.4	340	1	3	1c	5	Possible	4	Possible	Between Sm and AK
BBG-134	B134	1.3	123.6	260	2	2	0	4	Possible	4	Possible	Between AK and Me
BBG-135	B135	−0.8	131.6	200	2	2	0	4	Possible	4	Possible	Between AK and Me
BBG-136	B136	3.5	167.2	220	1	3	0	4	Possible	4	Possible	Cluster 29 around TOPO-19
BBG-137	B137	−1.8	168.4	320	2	3	0	5	Possible	5	Distinct	Cluster 29 around TOPO-19
BBG-138	B138	−5.3	176.5	160	2	2	0	4	Possible	4	Possible	
BBG-139	B139	−5.0	183.4	200	1	2	0	3	Possible	3	Possible	
BBG-140	B140	−6.2	192.2	200	1	2	0	3	Possible	3	Possible	West of Ko
BBG-141	B141	−10.0	209.0	160	2	2	0	4	Possible	4	Possible	Southeast of Ko
BBG-142	B142	−12.1	214.8	240	2	2	0	4	Possible	4	Possible	
BBG-143	B143	−5.9	224.0	220	1	2	0	3	Possible	3	Possible	Southwest of He
BBG-144	B144	−13.3	250.7	320	1	3	0	4	Possible	4	Possible	East of TOPO-26 and TOPO-27
BBG-145	B145	−6.7	254.1	240	1	2	0	3	Possible	3	Possible	Northwest of Or
BBG-146	B146	−3.2	259.0	200	1	2	0	3	Possible	3	Possible	North of Or
BBG-147	B147	−3.6	265.7	280	1	3	1c	5	Possible	4	Possible	North of Or
BBG-148	B148	0.3	268.9	280	1	3	0	4	Possible	4	Possible	North of Or
BBG-149	B149	−4.6	273.5	260	1	2	0	3	Possible	3	Possible	North of Or
BBG-150	B150	−9.1	278.7	240	1	2	0	3	Possible	3	Possible	Northeast of Or
BBG-151	B151	−16.9	282.2	280	1	3	0	4	Possible	4	Possible	Between Or and TOPO-30
BBG-152	B152	12.2	296.6	200	1	2	0	3	Possible	3	Possible	
BBG-153	B153	−12.9	308.5	420	1	3	1c	5	Possible	4	Possible	Between Cr, Hu, TOPO-30, and TOPO-35
BBG-154	B154	−20.2	304.3	340	1	3	1c	5	Possible	4	Possible	Between TOPO-30 and Hu
BBG-155	B155	−11.4	324.5	220	1	2	0	3	Possible	3	Possible	Cluster 30 around TOPO-30, north of Hu
BBG-156	B156	−4.7	326.2	240	1	2	0	3	Possible	3	Possible	Cluster 30 around TOPO-30, north of Hu
BBG-157	B157	−9.4	335.8	240	2	2	0	4	Possible	4	Possible	Cluster 30 around TOPO-30, north of Hu
BBG-158	B158	−13.7	331.6	360	2	3	0	5	Possible	5	Distinct	Cluster 30 around TOPO-30, north of Hu
BBG-159	B159	−1.5	350.9	260	1	2	0	3	Possible	3	Possible	Cluster 31
BBG-160	B160	−7.7	348.7	260	1	2	1c	4	Possible	3	Possible	Cluster 31
BBG-161	B161	−14.2	352.4	320	2	3	0	5	Possible	5	Distinct	Cluster 31; northeast of Nu
BBG-162	B162	−9.9	12.8	320	2	3	1c	6	Possible	5	Distinct	Between Ne, WA, and TOPO-2
BBG-163	B163	−18.8	13.4	360	2	3	1c	6	Possible	5	Distinct	Between Ne, WA, and TOPO-2
BBG-164	B164	−25.6	19.6	340	1	2	0	3	Possible	3	Possible	Between Ne and WA
BBG-165	B165	−29.3	28.6	260	2	3	0	5	Possible	5	Distinct	Between Ne and WA
BBG-166	B166	−20.8	55.0	400	1	3	1c	5	Possible	4	Possible	
BBG-167	B167	−27.1	81.4	240	1	2	3c	6	Possible	3	Possible	
BBG-168	B168	−16.6	89.3	240	2	3	0	5	Possible	5	Distinct	Cluster 32 south of Sm
BBG-169	B169	−17.8	96.0	180	1	2	3nc	6	Possible	3	Possible	Cluster 32 south of Sm
BBG-170	B170	−11.6	104.8	280	1	2	3nc	6	Possible	3	Possible	Cluster 32 south of Sm
BBG-171	B171	−19.4	137.3	240	2	3	0	5	Possible	5	Distinct	South of TOPO-12
BBG-172	B172	−16.9	154.7	300	2	3	0	5	Possible	5	Distinct	Cluster 33, east-west band, around TOPO-18
BBG-173	B173	−21.3	159.6	280	2	3	0	5	Possible	5	Distinct	Cluster 33, east-west band, around TOPO-18
BBG-174	B174	−18.7	165.4	260	2	3	0	5	Possible	5	Distinct	Cluster 33, east-west band, around TOPO-18
BBG-175	B175	−22.2	175.0	300	1	2	0	3	Possible	3	Possible	Cluster 33, east-west band
BBG-176	B176	−21.9	184.9	220	1	3	2c	6	Possible	4	Possible	Cluster 33, east-west band
BBG-177	B177	−22.9	191.8	220	1	2	2c	5	Possible	3	Possible	Cluster 33, east-west band
BBG-178	B178	−18.9	194.2	260	1	3	2c	6	Possible	4	Possible	Cluster 33, east-west band, southeast of CTA-15
BBG-179	B179	−19.2	198.8	260	1	3	2c	6	Possible	4	Possible	Cluster 33, east-west band
BBG-180	B180	−24.6	200.9	180	2	2	2c	6	Possible	4	Possible	Cluster 33, east-west band
BBG-181	B181	−21.3	207.3	200	2	2	2c	6	Possible	4	Possible	Cluster 33, east-west band
BBG-182	B182	−21.3	233.1	760	1	2	2nc	5	Possible	3	Possible	
BBG-183	B183	−37.0	1.7	220	2	3	0	5	Possible	5	Distinct	
BBG-184	B184	−39.7	65.2	160	1	2	1c	4	Possible	3	Possible	Cluster 34
BBG-185	B185	−35.4	69.9	220	1	2	1c	4	Possible	3	Possible	Cluster 34
BBG-186	B186	−35.7	76.8	200	1	2	1c	4	Possible	3	Possible	Cluster 34
BBG-187	B187	−38.0	98.3	200	1	2	1c	4	Possible	3	Possible	Cluster 35, southeast of TOPO-17
BBG-188	B188	−34.6	104.0	200	1	2	1c	4	Possible	3	Possible	Cluster 35, southeast of TOPO-17
BBG-189	B189	−37.1	108.0	200	1	2	2c	5	Possible	3	Possible	Cluster 35, southeast of TOPO-17
BBG-190	B190	−36.2	120.7	180	1	2	0	3	Possible	3	Possible	

Table A1. (continued)

Basin Identification[a]					Band-Limited Bouguer Gravity							
Name	Symbol	Lat (°)	Lon (°)	D (km)	gr[b]	r[c]	tr[d]	Rating 1[e]		Rating 2[f]		Comments[g]
BBG-191	B191	−25.4	145.3	220	2	3	0	5	Possible	5	Distinct	Cluster 36
BBG-192	B192	−31.4	146.8	260	2	3	0	5	Possible	5	Distinct	Cluster 36, north of TOPO-13
BBG-193	B193	−33.6	153.2	200	2	3	0	5	Possible	5	Distinct	Cluster 36, north of TOPO-13
BBG-194	B194	−38.1	179.3	260	1	2	3nc	6	Possible	3	Possible	Cluster 37 between In and Ap
BBG-195	B195	−33.3	186.8	220	1	2	1c	4	Possible	3	Possible	Cluster 37 between In and Ap
BBG-196	B196	−35.3	193.9	220	1	3	1c	5	Possible	4	Possible	Cluster 37 between In and Ap
BBG-197	B197	−40.9	189.4	200	1	2	3c	6	Possible	3	Possible	Cluster 37 between In and Ap
BBG-198	B198	−28.4	250.9	280	2	3	2c	7	Distinct	5	Distinct	Cluster 38 between Or and CTA-19
BBG-199	B199	−32.9	254.1	200	0	2	1c	3	Possible	2	Possible	Cluster 38 between Or and CTA-19
BBG-200	B200	−36.3	252.8	180	1	3	0	4	Possible	4	Possible	Cluster 38 between Or and CTA-19
BBG-201	B201	−37.9	259.2	200	1	3	0	4	Possible	4	Possible	Cluster 38 between Or and CTA-19
BBG-202	B202	−35.2	262.3	220	1	3	0	4	Possible	4	Possible	Cluster 38 between Or and CTA-19
BBG-203	B203	−36.0	274.0	400	2	3	0	5	Possible	5	Distinct	Between Or and MR
BBG-204	B204	−29.3	280.3	240	1	2	0	3	Possible	3	Possible	Southeast of Or
BBG-205	B205	−30.9	306.2	360	2	3	0	5	Possible	5	Distinct	Southwest of Hu
BBG-206	B206	−38.3	311.1	200	1	3	0	4	Possible	4	Possible	Southwest of Hu
BBG-207	B207	−39.8	320.7	220	1	2	0	3	Possible	3	Possible	South of Hu
BBG-208	B208	−25.2	337.7	220	1	2	0	3	Possible	3	Possible	Between Hu and Nu
BBG-209	B209	−23.7	350.1	400	2	3	2c	7	Distinct	5	Distinct	Southeast of Nu
BBG-210	B210	−34.3	332.0	320	1	2	1nc	4	Possible	3	Possible	Cluster 39 southeast of Nu
BBG-211	B211	−40.0	334.4	200	1	2	1c	4	Possible	3	Possible	Cluster 39 southeast of Nu
BBG-212	B212	−38.8	342.2	180	1	2	1c	4	Possible	3	Possible	Cluster 39 southeast of Nu
BBG-213	B213	−32.7	354.5	260	3	2	2c	7	Distinct	5	Distinct	
BBG-214	B214	−45.9	2.7	180	1	2	0	3	Possible	3	Possible	
BBG-215	B215	−42.8	34.4	220	2	2	0	4	Possible	4	Possible	
BBG-216	B216	−58.3	55.9	200	1	2	1nc	4	Possible	3	Possible	Cluster 40
BBG-217	B217	−54.7	63.7	220	1	2	1c	4	Possible	3	Possible	Cluster 40
BBG-218	B218	−54.3	76.1	180	2	2	1nc	5	Possible	4	Possible	Cluster 40
BBG-219	B219	−47.6	93.3	200	2	2	0	4	Possible	4	Possible	Northwest of Au
BBG-220	B220	−48.3	114.0	160	1	2	2c	5	Possible	3	Possible	Cluster 41 around TOPO-9
BBG-221	B221	−53.0	114.7	180	1	2	1c	4	Possible	3	Possible	Cluster 41 around TOPO-9
BBG-222	B222	−54.8	122.5	160	1	3	1c	5	Possible	4	Possible	Cluster 41 around TOPO-9
BBG-223	B223	−49.0	131.8	140	2	2	0	4	Possible	4	Possible	Cluster 42
BBG-224	B224	−45.3	133.9	160	2	2	0	4	Possible	4	Possible	Cluster 42
BBG-225	B225	−40.1	138.7	240	1	2	1c	4	Possible	3	Possible	Southeast of CTA-12
BBG-226	B226	−45.9	147.4	200	1	2	1c	4	Possible	3	Possible	
BBG-227	B227	−41.6	158.2	260	2	3	2nc	7	Distinct	5	Distinct	Southwest of In
BBG-228	B228	−48.1	175.6	220	3	3	2c	8	Distinct	6	Distinct	
BBG-229	B229	−47.0	216.5	140	2	2	1c	5	Possible	4	Possible	
BBG-230	B230	−39.7	228.8	180	1	3	2c	6	Possible	4	Possible	Cluster 43 between Ap and MR
BBG-231	B231	−44.0	232.6	200	1	3	2c	6	Possible	4	Possible	Cluster 43 between Ap and MR
BBG-232	B232	−44.2	238.7	220	1	3	2c	6	Possible	4	Possible	Cluster 43 between Ap and MR
BBG-233	B233	−48.7	233.3	160	1	3	2c	6	Possible	4	Possible	Cluster 43 between Ap and MR
BBG-234	B234	−50.6	241.2	180	1	3	2c	6	Possible	4	Possible	Cluster 43 between Ap and MR
BBG-235	B235	−53.6	235.6	180	1	3	2c	6	Possible	4	Possible	Cluster 43 between Ap and MR
BBG-236	B236	−45.3	289.4	160	3	2	0	5	Possible	5	Distinct	Cluster 44 between MR and SZ
BBG-237	B237	−51.2	291.1	220	1	2	1c	4	Possible	3	Possible	Cluster 44 between MR and SZ
BBG-238	B238	−50.0	299.2	180	2	3	0	5	Possible	5	Distinct	Cluster 44 between MR and SZ
BBG-239	B239	−55.0	293.9	180	1	2	1c	4	Possible	3	Possible	Cluster 44 between MR and SZ
BBG-240	B240	−60.6	297.9	140	1	2	1c	4	Possible	3	Possible	Cluster 44 between MR and SZ
BBG-241	B241	−54.8	337.1	200	1	2	0	3	Possible	3	Possible	Cluster 45
BBG-242	B242	−52.4	344.1	180	1	2	0	3	Possible	3	Possible	Cluster 45
BBG-243	B243	−65.2	20.7	160	1	2	1c	4	Possible	3	Possible	Cluster 46
BBG-244	B244	−71.0	26.0	140	1	2	1c	4	Possible	3	Possible	Cluster 46
BBG-245	B245	−69.2	37.3	180	1	2	1nc	4	Possible	3	Possible	Cluster 46
BBG-246	B246	−63.8	39.5	120	2	2	1c	5	Possible	4	Possible	Cluster 46
BBG-247	B247	−63.5	91.6	300	2	2	1c	5	Possible	4	Possible	Cluster 47 between Au and SR
BBG-248	B248	−59.4	104.3	200	2	2	1c	5	Possible	4	Possible	Cluster 47 between Au and SR
BBG-249	B249	−62.0	117.2	120	1	2	0	3	Possible	3	Possible	Between SR and Pl
BBG-250	B250	−59.9	148.0	140	1	3	1c	5	Possible	4	Possible	Cluster 48 between Pl and Po
BBG-251	B251	−64.7	143.2	160	1	2	1nc	4	Possible	3	Possible	Cluster 48 between Pl and Po
BBG-252	B252	−67.2	150.3	120	1	2	1c	4	Possible	3	Possible	Cluster 48 between Pl and Po
BBG-253	B253	−60.2	184.0	160	1	2	0	3	Possible	3	Possible	South of SA
BBG-254	B254	−57.9	206.0	160	1	2	1nc	4	Possible	3	Possible	Cluster 49 southeast of TOPO-23
BBG-255	B255	−61.5	203.1	140	1	2	1c	4	Possible	3	Possible	Cluster 49 southeast of TOPO-23
BBG-256	B256	−66.1	199.3	240	2	2	1c	5	Possible	4	Possible	Cluster 49 southeast of TOPO-23; joins cluster 50
BBG-257	B257	−73.0	202.8	160	1	2	1c	4	Possible	3	Possible	Cluster 50 southeast of TOPO-21; joins cluster 49
BBG-258	B258	−78.0	208.7	100	1	2	1c	4	Possible	3	Possible	Cluster 50 southeast of TOPO-21
BBG-259	B259	−82.1	216.1	100	1	2	1c	4	Possible	3	Possible	Cluster 50 southeast of TOPO-21

Table A1. (continued)

Basin Identification[a]					Band-Limited Bouguer Gravity							
Name	Symbol	Lat (°)	Lon (°)	*D* (km)	gr[b]	*r*[c]	tr[d]	Rating 1[e]		Rating 2[f]		Comments[g]
BBG-260	B260	−83.1	185.9	140	1	2	0	3	Possible	3	Possible	Cluster 50 southeast of TOPO-21
BBG-261	B261	−77.9	183.4	140	1	2	1nc	4	Possible	3	Possible	Cluster 50 southeast of TOPO-21
BBG-262	B262	−74.7	170.9	180	1	2	1c	4	Possible	3	Possible	Cluster 50 southeast of TOPO-21
BBG-263	B263	−60.9	258.5	180	1	2	0	3	Possible	3	Possible	Cluster 51 southwest of MR
BBG-264	B264	−63.6	249.7	240	1	2	1nc	4	Possible	3	Possible	Cluster 51 southwest of MR
BBG-265	B265	−67.0	240.7	160	1	2	1c	4	Possible	3	Possible	Cluster 51 southwest of MR
BBG-266	B266	−72.3	246.8	100	1	3	0	4	Possible	4	Possible	Cluster 51 southwest of MR
BBG-267	B267	−76.6	242.2	80	1	3	0	4	Possible	4	Possible	Cluster 51 southwest of MR
BBG-268	B268	−71.2	274.0	140	2	2	2c	6	Possible	4	Possible	
BBG-269	B269	−61.0	277.4	200	2	2	1c	5	Possible	4	Possible	South of PH
BBG-270	B270	−62.7	320.7	160	1	2	0	3	Possible	3	Possible	Southeast of SZ
BBG-271	B271	−69.7	344.1	100	2	2	1c	5	Possible	4	Possible	
BBG-272	B272	−62.1	358.1	140	1	2	1c	4	Possible	3	Possible	
BBG-273	B273	−77.9	36.1	120	1	2	2c	5	Possible	3	Possible	Cluster 52
BBG-274	B274	−74.8	51.1	180	1	2	2c	5	Possible	3	Possible	Cluster 52
BBG-275	B275	−81.4	59.5	100	1	2	0	3	Possible	3	Possible	Cluster 52
BBG-276	B276	−76.5	79.6	160	2	2	2c	6	Possible	4	Possible	Cluster 53 southwest of SR
BBG-277	B277	−73.7	95.0	160	2	3	2c	7	Distinct	5	Distinct	Cluster 53 southwest of SR
BBG-278	B278	−85.6	277.7	100	3	2	2c	7	Distinct	5	Distinct	
BBG-279	B279	−78.6	308.7	260	1	3	2c	6	Possible	4	Possible	Cluster 54
BBG-280	B280	−77.6	330.2	160	1	2	0	3	Possible	3	Possible	Cluster 54

[a]Name reflects band-limited Bouguer gravity (BGG). Longitude is given as eastern longitude. Rim diameter *D* is approximated to the nearest 20 km and is based on the spatial extent of the topographic signature or on the gravity signature in case no topographic signature is present (e.g., tr = 0).

[b]Gravity ring structure: (0) not present; (1) present to some extent; (2) present to considerable extent; (3) clearly present.

[c]Range (max minus min) over the basin: (0) $<$50 mGal; (1) 50–100 mGal; (2) 100–150 mGal; (3) $>$150 mGal.

[d]Topographic rim structure: (0) not visible; (1) visible to some extent; (2) visible to a considerable extent; (3) clearly visible. The letter c indicates that the gravity ring structure is centred over the topographic rim structure, while the letters nc indicate that it is not centred.

[e]Rating 1 (based on the sum of pr, *r*, and tr): (0–2) doubtful; (3–6) possible; (7–9) distinct.

[f]Rating 2 (based on the sum of pr and *r*): (0–1) doubtful; (2–4) possible; (5–6) distinct.

[g]Cluster indicates multiple-impact region with partly overlapping gravity and topography signals. Reference to existing impact basins indicates their closeness to the identified signal; names and abbreviations used refer to those in Table 2.

[38] **Acknowledgments.** We would like to thank the Australian Research Council for funding through discovery project grants DP0663020 and DP120102441. We also thank the model producers for making their lunar gravity field and topography models freely available. We are grateful to three anonymous reviewers for their thorough reviews and attention to detail, and to the Editor, Mark Wieczorek, for handling our manuscript and suggesting the whole-of-Moon analysis. Some of the figures were produced using GMT [*Wessel and Smith*, 1998]. This is the Institute for Geoscience Research (TIGeR) publication 471.

References

Bowin, C. (1983), Depth of principal mass anomalies contributing to Earth's geoid undulations and gravity anomalies, *Mar. Geod.*, *7*(1-4), 61–100, doi:10.1080/15210608309379476.

Floberghagen, R. (2002), *Lunar Gravimetry—Revealing the Far-Side*, Astrophys. and Space Sci. Libr., Kluwer Acad., Dordrecht, Netherlands.

Frey, H. V. (2011), Previously unknown large impact basins on the Moon: Implications for lunar stratigraphy, *Spec. Pap. Geol. Soc. Am.*, *477*, 53–75, doi:10.1130/2011.2477(02).

Frey, H. V., B. G. Bills, and R. S. Nerem (1996), The isostatic state of Martian topography revisited, *Geophys. Res. Lett.*, *23*(7), 721–724, doi:10.1029/96GL00744.

Goossens, S., et al. (2011), Lunar gravity field determination using SELENE same-beam differential VLBI tracking data, *J. Geod.*, *85*(4), 205–228, doi:10.1007/s00190-010-0430-2.

Griffin, W. R. (1949), Residual gravity in theory and practice, *Geophysics*, *14*(1), 39–56, doi:10.1190/1.1437506.

Hackney, R. I., and W. E. Featherstone (2003a), Geodetic versus geophysical perspectives of the "gravity anomaly," *Geophys. J. Int.*, *154*(1), 35–43, doi:10.1046/j.1365-246X.2003.01941.x.

Hackney, R. I., and W. E. Featherstone (2003b), Erratum, *Geophys. J. Int.*, *154*(2), 596, doi:10.1046/j.1365-246X.2003.02058.x.

Hackney, R. I., and W. E. Featherstone (2006), Corrigendum, *Geophys. J. Int.*, *167*(2), 585, doi:10.1111/j.1365-246X.2006.03035.x.

Han, S.-C. (2008), Improved regional gravity fields on the Moon from Lunar Prospector tracking data by means of localized spherical harmonic functions, *J. Geophys. Res.*, *113*, E11012, doi:10.1029/2008JE003166.

Hirt, C. (2012), Efficient and accurate high-degree spherical harmonic synthesis of gravity field functionals at the Earth's surface using the gradient approach, *J. Geod.*, *86*(9), 729–744, doi:10.1007/s00190-012-0550-y.

Huang, Q., and M. A. Wieczorek (2012), Density and porosity of the lunar crust from gravity and topography, *J. Geophys. Res.*, *117*, E05003, doi:10.1029/2012JE004062.

Huang, Q., J. S. Ping, X. L. Su, R. Shu, and G. S. Tang (2009), New features of the Moon revealed and identified by CLTM-s01, *Sci. China, Ser. G*, *52*(12), 1815–1823, doi:10.1007/s11433-009-0284-x.

Kiefer, W. S., R. J. Macke, D. T. Britt, A. J. Irving, and G. J. Consolmagno (2012), The density and porosity of lunar rocks, *Geophys. Res. Lett.*, *39*, L07201, doi:10.1029/2012GL051319.

Konopliv, A. S., S. W. Asmar, E. Carranza, W. L. Sjogren, and D. N. Yuan (2001), Recent gravity models as a result of the Lunar Prospector mission, *Icarus*, *150*(1), 1–18, doi:10.1006/icar.2000.6573.

Matsumoto, K., et al. (2010), An improved lunar gravity field model from SELENE and historical tracking data: Revealing the far-side gravity features, *J. Geophys. Res.*, *115*, E0600, doi:10.1029/2009JE003499.

Muller, P., and W. Sjogren (1968), MASCONS—Lunar mass concentrations, *Science*, *161*(3842), 680–684, doi:10.1126/science.161.3842.680.

Namiki, N., et al. (2009), Far-side gravity field of the Moon from four-way Doppler measurements of SELENE (Kaguya), *Science*, *323*(5916), 900–905, doi:10.1126/science.1168029.

Nettleton, L. L. (1954), Regionals, residuals, and structures, *Geophysics*, *19*(1), 143–156, doi:10.1190/1.1437966.

Neumann, G. A., M. T. Zuber, D. E. Smith, and F. G. Lemoine (1996), The lunar crust: Global structure and signature of major basins, *J. Geophys. Res.*, *101*(E7), 16,841–16,863, doi:10.1029/96JE01246.

Reindler, L., and J. Arkani-Hamed (2001), The compensation state of intermediate size lunar craters, *Icarus*, *153*, 71–88, doi:10.1006/icar.2001.6677.

Rummel, R., R. H. Rapp, H. Sünkel, and C. C. Tscherning (1988), Comparisons of global topographic/isostatic models to the Earth's observed gravity field, *Rep. 388*, Dep. of Geod. Sci. and Surv., Ohio State Univ., Columbus.

Sinha, M., N. S. Gopinath, and N. K. Malik (2010), Lunar gravity field modeling: Critical analysis and challenges, *Adv. Space Res.*, *45*(2), 322–349, doi:10.1016/j.asr.2009.10.006.

Sjöberg, L. E. (2007), The topographic bias by analytical continuation in physical geodesy, *J. Geod.*, *81*(5), 345–350, doi:10.1007/s00190-006-0112-2.

Smith, D. E., M. T. Zuber, G. A. Neumann, and F. G. Lemoine (1997), Topography of the Moon from the Clementine LIDAR, *J. Geophys. Res.*, *102*(E1), 1591–1611, doi:10.1029/96JE02940.

Smith, D. E., et al. (2010), Initial observations from the Lunar Orbiter Laser Altimeter (LOLA), *Geophys. Res. Lett.*, *37*, L18204, doi:10.1029/2010GL043751.

Sugano, T., and K. Heki (2004), Isostasy of the Moon from high-resolution gravity and topography data: Implication for its thermal history, *Geophys. Res. Lett.*, *31*, L24703, doi:10.1029/2004GL022059.

Vondrak, R., J. Keller, G. Chin, and J. Garvin (2010), Lunar Reconnaissance Orbiter (LRO): Observations for lunar exploration and science, *Space Sci. Rev.*, *150*(1-4), 7–22, doi:10.1007/s11214-010-9631-5.

Wessel, P., and W. H. F. Smith (1998), New, improved version of the generic mapping tools released, *Eos Trans. AGU*, *79*, 579, doi:10.1029/98EO00426.

Wieczorek, M. A. (2007), Gravity and topography of the terrestrial planets, in *Treatise on Geophysics*, vol. 10, edited by T. Spohn and G. Schubert, pp. 165–206, Elsevier, Oxford, U. K.

Wieczorek, M. A., and M. Le Feuvre (2009), Did a large impact reorient the Moon?, *Icarus*, *200*, 358–366, doi:10.1016/j.icarus.2008.12.017.

Wieczorek, M. A., and R. J. Phillips (1998), Potential anomalies on the sphere: Applications to the thickness of the lunar crust, *J. Geophys. Res.*, *103*(E1), 1715–1724, doi:10.1029/97JE03136.

Wieczorek, M. A., et al. (2006), The constitution and structure of the lunar interior, *Rev. Mineral. Geochem.*, *60*(1), 221–364, doi:10.2138/rmg.2006.60.3.

Wieczorek, M. A., et al. (2013), The crust of the Moon as seen by GRAIL, *Science*, *339*(6120), 671–675, doi:10.1126/science.1231530.

Wood, C. (2004), Impact Basin Database. [Available online at: http://www.lpod.org/cwm/DataStuff/Lunar%20Basins.htm.]

Zuber, M. T., et al. (2013), Gravity field of the Moon from the Gravity Recovery and Interior Laboratory (GRAIL) mission, *Science*, *339*(6120), 668–671, doi:10.1126/science.1231507.